Aus dem

Lehrstuhl für Physiologische Chemie, Biomedizinisches Centrum (BMC) Institut der Ludwig-Maximilians-Universität München



Mettl3 is required cell intrinsically in both muscle and neurons for development of functional flight muscle

Dissertation

zum Erwerb des Doktorgrades der Medizin an der Medizinischen Fakultät der Ludwig-Maximilians-Universität München

vorgelegt von

Jakob Heemken

Im Jahr

2025

Mit Genehmigung der Medizinischen Fakultät der Ludwig-Maximilians-Universität zu München

Erstes Gutachten: Prof. Dr. Andreas G. Ladurner

Zweites Gutachten: Prof. Dr. Michael Kiebler

Drittes Gutachten: Prof. Dr. John Parsch

Dekan: Prof. Dr. med. Thomas Gudermann

Tag der mündlichen Prüfung: 19.09.2025

Table of contents 3

Table of contents

| Table (| of contents | 3 | | |
|----------------------|---|----|--|--|
| Zusam | menfassung: | 5 | | |
| Abstract (English):7 | | | | |
| 1. | Introduction | 9 | | |
| 2. | Material and Methods | 15 | | |
| 2.1 | Drosophila husbandry | 15 | | |
| 2.2 | Behavioural tests | 16 | | |
| 2.2.1 | Flight test | 16 | | |
| 2.2.2 | Climbing test | 16 | | |
| 2.2.3 | Wing angle assay | 17 | | |
| 2.3 | Imaging | 17 | | |
| 2.3.1 | Sample preparation | 17 | | |
| 2.3.2 | Immunohistochemistry | 17 | | |
| 2.3.3 | Confocal microscopy | 18 | | |
| 2.4 | Biochemical procedures | 19 | | |
| 2.4.1 | Western blot | 19 | | |
| 2.4.2 | Dot blot | 19 | | |
| 2.4.3 | qPCR | | | |
| 2.4.4 | RT-PCR | | | |
| 2.4.5 | Proteomics (Mass Spectrometry) | | | |
| 2.4.6 | Transcriptomics (mRNA-Seq). | 23 | | |
| 2.5 | Data processing | 24 | | |
| 3. | Results | 25 | | |
| 3.1 | Behavioral assays | 25 | | |
| 3.1.1 | Flies lacking the Mettl3 methylase are flightless and exhibit motor deficits | 25 | | |
| 3.1.2 | Mettl3 is expressed and functionally active in both brain and IFM | 25 | | |
| 3.1.3 | • | 26 | | |
| 3.1.4 | Tissue-selective knockdown of Mettl3 using RNAi in muscle or neurons | | | |
| 3.1.5 | Muscle-specific Mettl3 knockdown results in flightlessness | | | |
| 3.1.6 | Sarcomeres in muscle-specific knockdown IFM show defects | 34 | | |
| 3.1.7 | Tissue-specific expression of Mettl3 is unable to rescue mutant behavioural phenotypes | 37 | | |
| 3.1.8 | Muscle-specific Mettl3 expression can rescue the sarcomere phenotype | | | |
| 3.1.9 | Sarcomere proteins are misregulated in Mettl3 RNAi IFM | | | |
| 3.1.10 | • | | | |
| 3.1.11 | Proteomic analysis of Mettl3 mutant IFMs | 46 | | |
| 3.2 | Neuronal structure | 49 | | |
| 3.3 | mRNA-Seq analysis | 52 | | |
| 3.3.1 | mRNA sequencing revealed altered transcriptional patterns of muscle related genes in <i>Mettl3</i> mutant flies | | | |
| 3.3.2 | Decreased expression of Mettl3 causes changes in mRNA levels of muscle relate proteins | | | |

Table of contents 4

| 3.3.3 | Decreased expression of Mettl3 in an increase in the mRNAs of neuronal- and synaptic related proteins | 56 |
|--------------|---|----|
| 3.3.4 | Decreased expression of Mettl3 causes defects in alternative splicing and isofor expression of Titin-like protein Projectin | |
| 4. | Discussion | 61 |
| 4.1 | Flightlessness of Mettl3 mutants is not a purely neuronal phenotype | 61 |
| 4.2 | Mettl3 is required in muscle to regulate sarcomere dimensions in IFM | 62 |
| 4.3 | Mettl3 and the m6A pathway regulate alternative splicing in IFM | 63 |
| 4.4 | mRNA transcript-level changes in Mettl3 mutant IFM are reflected in the proteon | |
| 4.5 | Conclusion | 65 |
| References68 | | |
| Appendix | | 73 |
| Ackno | owledgements | 76 |
| Confi | rmation of congruency | 77 |
| Public | rations | 78 |

Zusammenfassung: 5

Zusammenfassung:

Die Entwicklung von Muskelgewebe ist ein hochkomplexer Prozess. Durch alternatives Spleißen und präzise Regulation der Genexprimierung zeigt dieses Gewebe sowohl zeitlich wie räumlich unterschiedliche Expressionsmuster von Isoformen seiner Gene. Über diese Mechanismen werden die physiologische Entwicklung der Sarkomere sowie ihre fein abgestimmten kontraktilen Eigenschaften realisiert. In Krankheiten wie Muskeldystrophie und Kardiomyopathien lässt sich eine Missregulation in der Exprimierung von Genisoformen beobachten. Daraus wird ersichtlich, warum es von Interesse ist diese Vorgänge zu erforschen und zu verstehen.

N6-Methyladenosin ist eine Modifikation der RNA von der man annimmt, dass sie viele physiologische Funktionen in der RNA Prozessierung übernimmt. Dazu zählen alternatives Spleißen, Stabilisierung der mRNA, Export und Translation. Dennoch bleiben viele Funktionen dieser Modifikationen bis heute unklar.

Kernelemente des zugehörigen m6A-Signalwegs wie Mettl3 und Mettl14 sind evolutionär hoch konserviert. Dieser Umstand erlaubt es potente genetische Werkzeuge, wie sie in Modellorganismen wie *Drosophila Melanogaster* verfügbar sind, einzusetzen. So können die Funktionen dieses evolutionär sehr alten Signalwegs in vivo näher beleuchtet werden.

In der vorliegenden Arbeit werde ich zeigen, dass Mettl3 eine wichtige Rolle bei der Entwicklung der indirekten Flugmuskulatur (IFM) und ihrer zugehörigen Motorneurone spielt.

Ein kompletter Verlust des essenziellen Enzyms Mettl3 in mutierten Fliegen führt zur Flugunfähigkeit und zu herabgesetzter Klettergeschwindigkeit. Konfokale Mikroskopie zeigte veränderte physikalische Dimensionen der IFM wie auch erhöhte Verzweigungsraten der Motoneurone. Mit Hilfe Muskel spezifischer RNAiknockdowns konnten wir zeigen, dass ein Ausfall von Mettl3 im Muskelgewebe zu Flugunfähigkeit und zu veränderten Abmessungen der Sarkomere führt. Ein Ausfall von Mettl3 in neuronalem Gewebe hingegen offenbarte Defekte in der Verzweigung der Motoneurone.

Zusammenfassung: 6

Die veränderten Abmessungen im Muskel konnten durch die muskelspezifische Exprimierung von Mettl3 mittels Mef2-Gal4 in einem ansonsten globalen Mettl3 Knockdown geheilt werden. Analog dazu ließen sich die Verzweigungsdefekte durch Exprimierung von Mettl3 durch Elav-Gal4 nur in Neuronen beheben.

Aus diesen Erkenntnissen lässt sich eine muskel- und eine neuronenspezifische Aktivität von Mettl3 ableiten.

Mittels mRNA-Sequenzierung und qPCR zeigen wir, dass IFM, denen Mettl3 fehlt, veränderte Expressionsmuster von Genen zeigt, die in Verbindung zu Sarkomeren, Mitochondrien und Synapsen stehen. Im Zuge einer proteomweiten Massenspektrometrie und durch Experimente mit GFP-reportern fielen viele dieser Gene ebenfalls durch veränderte Expression auf.

Interessanterweise offenbarten unsere Experimente weiter signifikante Veränderungen im alternativen Spleißen muskelassoziierter Gene. Hier wurden unter anderem Isoformenwechsel der Titin ähnlichen Gene *bent* (bt, Projectin), *Myofilin* (Mf), *Zasp52* und *Unc-89* beobachtet.

Diese Daten bestätigen eine muskelspezifische Aktivität der m6A-Modifikation. Die Modifikation ist somit beteiligt in der Regulierung des alternativen Spleißens und der Exprimierung von muskelassoziierten Genen, die für die physiologische Entwicklung der Muskelfibrillen erforderlich sind.

Abstract (English): 7

Abstract (English):

Muscle development is a highly organized and complex process. Through the precise regulation of gene expression and alternative splicing, muscles define temporal and spatial patterns of gene isoform expression that promote sarcomere assembly and fine-tune contractile properties. Misregulation of gene isoform expression is observed in diseases ranging from muscular dystrophies to cardiomy-opathies, illustrating the importance of understanding this process. N6-Methyladenosine (m6A) is an RNA modification that is suggested to regulate multiple steps in RNA processing, including alternative splicing, mRNA stability, trafficking and translation efficiency, but many of its cellular functions still remain elusive. Core enzymes in the m6A-pathway such as Mettl3 and Mettl14 are highly conserved, providing the opportunity to utilize powerful genetic tools available in model organisms such as *Drosophila melanogaster* to understand *in vivo* functions of this ancient pathway. In this thesis, I show that Mettl3 plays an important role in the development of both the indirect flight muscles (IFMs) and their corresponding motor neurons.

Complete loss of the essential enzyme Mettl3 in mutant flies results in flightlessness and impaired climbing ability. Confocal imaging revealed altered sarcomere
dimensions in IFM, as well as extensive over-branching of motor neurons. Using
tissue-specific RNAi knockdown, we found that muscle-specific Mettl3 knockdown flies are flightless and have defects in sarcomere length, while neuronalspecific Mettl3 knockdown flies have defects in motor neuron branching. Sarcomere length defects could be rescued selectively by expression of Mettl3 with
Mef2-Gal4 in muscle, while neuronal defects could be rescued selectively by expression of Mettl3 with Elav-Gal4 in neurons. This indicates muscle and neuronintrinsic Mettl3 function. Using mRNA-Sequencing and qPCR, we show that IFM
lacking Mettl3 has changes in gene expression of sarcomere, mitochondrial and
synapse-associated genes, many of which are also misexpressed on the protein
level as detected by whole-proteome mass spectrometry and GFP-tagged reporters.

Abstract (English): 8

Strikingly, our experiments revealed significant changes in muscle specific alternative splicing, including isoform switches in key sarcomere proteins such as the Titin-like gene *bent* (*bt*, Projectin), *Myofilin* (Mf), *Zasp52* and *Unc-89*. This data confirms a muscle-intrinsic function for m6A modification in regulating alternative splicing and protein expression levels during myofibrillogenesis that is necessary for proper growth in sarcomere length and muscle function.

1. Introduction

Muscle is a highly conserved tissue that is found in all animals. Muscle facilitates movement, and although different species develop multiple different types of muscle fibres, the smallest contractile unit of muscle, the sarcomere, can be found in all of them [1]. The main building blocks of sarcomeres are the proteins actin and myosin. Actin filaments, or thin filaments, are arranged in a cylindrical shape around piston shaped myosin filaments (or thick filaments), and densely packed in a hexagonal pattern to fill the available space as effective as possible [2]. Two actin filaments are anchored in opposite directions at the z-disc, while bipolar myosin filaments are anchored at the M-line. Interleaving of the thin and thick filaments at the A-band allows myosin to move along actin towards the z-disc, causing the structure to contract. Sarcomeres are organized end-to-end into long myofibrils, which span the length of the muscle.

The development of muscle tissue is a highly organized process. It starts with the presence of myoblasts, which are muscle precursor cells [1, 3]. During development, these myoblasts will migrate to sites of muscle formation and fuse to form a large syncytial myotube [4]. Myotubes grow and connect to tendon cells, providing the tension necessary for the assembly of myofibrils [5, 6]. Those fibrils can reach lengths up to several centimeters in humans and even around one millimeter in fruit flies [7]. The pre-myofibril structure initially built in growing myofibers is remodelled during subsequent maturation, undergoing addition of more sarcomeres and exchange or addition of components to enable mature contractile dynamics [1]. Myogenesis is therefore characterized by distinct stages with distinct morphological and physiological characteristics that enable the step-wise assembly of fully-functional adult muscle tissue.

Muscle fibers will not develop identically in every part of the organism but rather differentiate into different muscle types with specific morphologies and functional properties. Vertebrate skeletal muscles consist of a mixture of fast and slow twitch fibers.

Fast twitch fibers are easily fatigued, while slow twitch fibers are more fatigue resistant [2, 8]. On a molecular level, these fiber types express different isoforms of myosin, giving a molecular basis for those differences in function.

Fast twitch fibers express the type II version of myosin, together with a gene expression program that influences the muscle towards a more glycolytic and faster metabolism [9]. The slow twitching fibers, on the contrary, express the type I myosin and have a more oxidative and slower, yet more fatigue resistant, metabolism. Interestingly, myofibers exist on a continuous spectrum between "fast" and "slow", and the muscle can adapt gene expression programs depending on physiologic need to fine-tune performance [10, 11]. Detailed reviews on muscle type identity and gene expression are available [9, 12], so I will not step into further detail here.

Like vertebrates, insects have different types of muscles and muscle fibers. In *Drosophila melanogaster* we can observe major architecture differences between tubular and fibrillar muscles, corresponding to synchronous and asynchronous muscles. Synchronous tubular muscles can be found all over the body of the animal, for example in its legs, abdomen or head. Here the fibers are organized around the nuclei in a peripheral, "tube-like" pattern [2, 13, 14]. Synchronous muscles are controlled by a corresponding nerve, and together they will form a unit [2, 13, 14]. Upon neuronal stimulation, calcium ions will be released. Those ions will then promote the cross-bridge cycle, causing the fibre to contract [2, 8, 9]. The ratio between neuronal input and muscle contraction here is 1:1.

On the other hand, the indirect flight muscles (IFM) that span across the thorax in regular bundles are fibrillar and asynchronous. Each fiber is a syncytial cell and the nuclei are arranged over the whole length of the fiber [6]. Asynchronous muscles, once initially activated by their nerve, can contract independently of neuronal input as they rely on a mechanical stretch-activation mechanism[14, 15].

This alternative mode of operation together with an increased stiffness due to a short titin isoform allows them to oscillate independently from neuronal input and at high frequencies with good power output [16, 17]. The transcription factor Spalt major (*salm*) is responsible for the fibrillar fate of the developing IFM, both through regulation of the fibrillar transcriptional program as well as by alternative splicing of genes and regulating the expression of those gene isoforms [12, 18, 19].

In vertebrates and in insects, distinct muscle fibers, for example heart or skeletal muscle, exhibit differences in mechanical properties like stiffness, in contractile properties including twitching speed and endurance, in general structural

architecture, and also in the neuronal control mechanism [9, 12, 17]. The mechanical differences are achieved by differential expression of muscle core components. Take for example Titin, a large protein with an extensible domain (PEVK-domain) that attaches the thick filaments to the thin filaments and z-disks and serves as the intermediate filament that determines sarcomere length, influences passive resting stiffness, and modulates contractile dynamics [20]. Long isoforms of this protein are found in skeletal muscles, dictating longer sarcomere lengths and lower resting stiffness, while shorter isoforms are found mammalian cardiomyocytes concurrent with shorter sarcomere lengths and a higher mechanical stiffness compared to skeletal muscles [21]. The pattern of isoform expression therefore underlies the morphological and contractile properties of muscle fiber types.

There are multiple mechanisms cells use to regulate the expression of different gene isoforms. In addition to the regulation of transcription, translation or protein stability, a lot of regulation occurs on the level of RNA. RNA is modified in multiple ways, for example through splicing, capping or editing for particular nucleotides [22]. In particular, alternative splicing allows one gene to code for many different isoforms of associated proteins, dramatically increasing the proteome diversity [23]. In addition, RNA modifications can affect the trafficking, localization, stability and translation rate of mRNA transcripts [24, 25], giving cells the possibility to finely tune their functions and development.

One of these RNA-modification pathways is the m6A pathway. With its two main components Mettl3 and Mettl14, the methyl-transferase complex can attach a methyl group to an adenosine base of a target RNA strand. This particular N6-methyladenosine RNA-modification is one of the most abundant found in mRNA in eukaryotic cells [26, 27]. In particular, this mark is enriched in 5'-UTRs, around stop codons and within long exons, often at the consensus sequence RRACH, where R stands for adenosine or guanine and H for adenosine, cytosine or uracil [27-29]. The m6A mark has been shown to influence fundamental biological processes such as RNA splicing, polyadenylation, nuclear export, stabilisation, translation and decay [22]. It has been shown to impact neuronal tissue development, notably axonal growth and synaptic structure, in *Drosophila* larva [30]. There are further reported functions in the differentiation of C2C12 myoblasts and heart development in vertebrates [31].

The detailed functions of the pathway are still incompletely understood, as only recent methodologies such as methylation-specific immunoprecipitation and next generation sequencing have made it possible to further investigate its functions [24].

The methyl-transferase complex consists of multiple components, including Mettl3 and Mettl14, as well as for example WTAP [FI(2)d], VIRMA (*Vir*), Zc3H13 (Flacc), RBM15, RBM15b (*Nito*) and HAKAI [29, 32, 33]. Mettl3 is the main enzyme responsible for methylation, or the "writer," which can catalyse the methylation reaction. Mettl14 is a key scaffolding component that stabilizes the complex, and other components are thought to guide the complex to its target sites [22, 26]. Although protein constituents of the complex can be diverse across the species, Mettl3 and Mettl14 are the core members and are highly conserved [34, 35]. Other proteins in the cell such as FTO and ALKBH5 are capable of removing the methyl mark and thus acting as "erasers". Comparable enzymes have not been identified yet outside of vertebrates, as FTO and ALKBH5 display poor sequence conservation across evolution [22, 36, 37].

The m6A mark can further be recognized by "reader" proteins, notably those containing the so called YTH-region, which are highly conserved. The presence of the mark increases the binding affinity of YTH-domain proteins 20- to 50-fold [22, 38, 39]. Reader proteins are reported to have distinct cytosolic or nuclear localisation patterns and to fulfil multiple tasks from mediating alternative splicing and RNA editing to directing mRNA transport, stability and translation dynamics [39, 40].

Since both "writer" and "reader" proteins are evolutionarily conserved, important insights into m6A pathway function as well as the discovery of novel pathway components have been reported in model organisms such as *Drosophila*. In this thesis, I explore the influence of the m6A pathway in muscle tissue *in vivo*, using *Drosophila melanogaster* as a model organism. In addition to conservation of the m6A pathway, *Drosophila melanogaster* is a well-established model organism in the field of genetics. Flies are easy to handle and they have a short generation time of 100 hours [41, 42]. They only have 4 chromosomes, which can be precisely manipulated with modern methods, and flies have a well-developed battery

of genetic tools such as the UAS/Gal4 system that permit precise control of spatial and temporal expression. *Drosophila* exhibits strong gene conservation with human genes, including 75% of all disease related genes, and has proven to be a useful model organism to understand conserved disease mechanisms [43]. Notably, muscle structure as well as the contractile mechanism of myosin-mediated contraction are well conserved, and *Drosophila* is also very suitable in the field of muscle studies [44]. *Drosophila melanogaster* is thus a suitable model organism for my project.

Development of the adult musculature, in particular the flight muscles, is well characterized in *Drosophila*. Two types of muscles are used for flight: the direct flight muscles (DFM) and the indirect flight muscles (IFM). The DFM are located in a fan like formation around the wing hinge and control the angle between the wings and the thorax. They are required for steering during flight and correct wing positioning [45]. DFM have a tubular muscle structure and are a synchronous muscle that respond to individual neuronal impulses.

The indirect flight muscles (IFM) consist of six large fibers that are spanning from anterior to posterior through the whole thorax (dorsolongitudinal muscles, DLM) and seven fibers, which span from the ventral to the dorsal side (dorsoventral muscles, DVM) [12]. IFM generate thrust by oscillating the thoracic cuticle, which causes the wings to move up and down. IFM have a distinct fibrillar structure and are asynchronous, meaning that their contractions are dissociated from neuronal impulses [12, 19]. Instead, a stretch-activation mechanism is employed to maintain the rapid, high-power contractions necessary to sustain flight [12, 19]. IFM has patterns of gene expression and alternative splicing that are distinct from those in tubular muscle [12, 19], and serve as a model system to test how regulation of gene expression and RNA processing contribute to muscle differentiation and contractility.

In this thesis project, I first demonstrate that Mettl3 mutant flies display defects in behavioural properties like flight, climbing and wing positioning. I show that Mettl3-/- IFM has a sarcomere phenotype, as well as underlying changes in gene and protein expression and alternative splicing, as assayed by whole-proteome mass spectrometry and mRNA-Seq, respectively. To define the tissue-specific requirement of Mettl3, I performed RNAi knockdown with the UAS/Gal4 system

specifically in muscle or neurons. My data show that Mettl3 is required in both tissues, as neuronal-specific RNAi leads to a severe motor neuron axon overbranching defect, while the sarcomere phenotype can be replicated by muscle-specific RNAi. Using RT-PCR, qPCR and GFP-tagged Fosmid reporters, our data demonstrates isoform-switches and misregulation of sarcomere gene expression, providing a possible mechanism to explain the observed structural and functional defects in IFM. I then perform tissue-specific rescue by expressing Mettl3 in a specific target tissue in the Mettl3 mutant background. My data thus demonstrate a novel, *in vivo* requirement for Mettl3 and m6A modification in muscle for the regulation of muscle-type specific sarcomere gene splicing and expression. Further, my results demonstrate that Mettl3 function in both muscle and neurons contribute to the observed behavioural defects.

2. Material and Methods

2.1 Drosophila husbandry

For this project I used *D. melanogaster* as a model organism. Fly work was performed with approval in Germany according to §15 GenTSV (license number 55.1-8791-14.1099). Fly stocks were maintained at room temperature using standard culture conditions. Experimental crosses were maintained at 18 °C, room temperature (~22 °C) or 27 °C, as noted. Fly food was prepared in a water-jacketed cooker by combining 16 L water, 150 g soy flour, 1.300 g corn flour, 300 g yeast, 130 g agar, 1.300 g molasses, and 650 g malt extract. After cooling, food was supplemented with 415 mL 10% Nipagin and 295 mL acid mix containing 3% phosphoric acid and 21% propionic acid. Food was aliquoted with a peristaltic pump, allowed to set at room temperature (RT) and stored at 4 °C until use.

The genotypes used in this study were: w^{1118} ;;; as wildtype (Bloomington stock number: 3605), y,w;; $Ime4^{\Delta 22-3}/TM3$, Ser (gift of M. Soller), ;; Df(3R)Exel6197(III) / Tm6b,Tb (Bloomington stock number 7676), ;Mef2-Gal4;; (gift of F. Schnorrer) [46]; Elav-Gal4/Cyo; (gift of L. Luo), Elav-Gal4/Cyo; Mef2-Gal4/Tm6.Tb (crossed by Shao-Yen Kao), UAS-Dcr2;;Mef2-Gal4/(TM3,Sb) (Gift of F. Schnorrer), ;If/Cyo; Sb/Tm3, Ser (gift of F. Schnorrer), UAS-Dcr2;; Ly/TM3, Sb (gift of F. Schnorrer), ;ElavGal4/Cyo; $Ime\Delta 22$ -3/TM3, Ser (crossed by Maria Spletter), ;UAS-Ime4/Cyo; Ime4Df/TM3, Ser

For the hairpins we used *Ime4 RNAis* (NIG stock number 5339-R, Bloomington stock numbers 80431, 80448, 80450, 41590 and VDRC stock number 20968). We also used *Mettl14 RNAis* (Bloomington stock number 64547 and VDRC stock numbers 48560, 105434, 38349) and *YT521-B RNAis* (Bloomington stock number 34627 and VDRC stock number 330558)

Furthermore we used GFP-tagged Fosmid lines inserted into attPVK33 available from VDRC including *Mef2-Gal4*, 876 fln::GFP (VK33), *Mef2-Gal4*, 501 Mf::GFP (VK33), *Mef2-Gal4*, 519 Mhc::GFP (VK33), *Mef2-Gal4*, 925 wupA::GFP (VK33), *Mef2-Gal4*, 78 Act88F::GFP (VK33), *Mef2-Gal4*, 500 Mhc::GFP (VK33), *Mef2-Gal4*, 477 sls::GFP (VK33), *Mef2-Gal4*, 478 Fhos::GFP (VK33), w*; P(UAS-GFP-FP4mito)119a and Mef2-Gal4,1046 unc-89::GFP (VK33) (all obtained from F. Schnorrer)

2.2 Behavioural tests

2.2.1 Flight test

Flight was tested with a tube made of acrylic glass. The tube itself was divided into 4 sections and had a little funnel at the very top of it. The flies to be tested were given into that funnel. Normal fliers would be found in the upper 2 sections, medium fliers in the lower 2 sections and finally flightless flies would fall straight to the bottom of the tube. The number of flies per test in each section was then counted [47]. At least 100 flies per genotype were assayed in groups of 20-30 flies, data were aggregated, and final results are reported as the percentage of total flies that were fliers, weak fliers, or flightless.

2.2.2 Climbing test

The climbing ability of the flies was tested using falcon tubes. Those tubes had a circular line in a 5 cm distance from the lid. Around 10 flies from a genotype to be tested were given into such a falcon tube. The tube was then sharply knocked on a hard surface, causing the flies to fall to the lid. Out of instinct, the flies inside start to crawl up the vial's walls immediately. This behaviour was recorded using the Open Camera application or a video recording application on a cell phone. The obtained video was then stopped at 3 seconds and at 5 seconds and the number of flies which made it above the 5 cm line in that time was recorded [46].

This assay was repeated 3 times for each sample group, with around 20 seconds of recovery time in between. Data are reported as the average of these three trials. At least 100 flies were tested in total for each genotype.

2.2.3 Wing angle assay

The wing angle of the flies was observed by observing groups of around 10 flies of a genotype. Normally those assays were made in parallel to the climbing assays. Flies which held out their wings were counted. At least 100 flies were observed, and data is reported as the percentage of total flies with held-out wings.

2.3 Imaging

2.3.1 Sample preparation

The myofibrillar structure and the motor neuron axonal branching pattern was analysed in adult thoraxes cut into halves longitudinally. The dissection was performed as described [5]. Neuronal tissue was analysed in whole adult brains. Tissues were dissected in 1x phosphate buffered saline (PBS), and then transferred to a buffer solution consisting of 1x PBS and 0.5% Triton-X100 (PBS-T) for permeabilization. All probes were fixed for ~25 mins in 4% paraformaldehyde at room temperature on a nutator. This step was followed by two 5-minute washing steps in PBS-T. Probes were stored a 4°C, or immediately stained as described below.

2.3.2 Immunohistochemistry

In this project, we used the following stains and antibodies: Rhodamine-Phalloidin (1:500, ThermoFisher) to stain actin, anti-horseradish peroxidase (HRP) 647 (1:100, ThermoFisher) to staining axon projections, rat anti-Kettin (1:100, MAC155/Klg16, Babraham Institute), guinea-pig anti-lme4 (Hongay and Orr-Weaver, PNAS, 2011) (1:100, gift of A. Rockwell),

rabbit anti-GFP antibody (1:1000, ab290, Abcam). Secondary antibodies from Invitrogen were used 1:100 and included Alexa 488 goat anti-rat (A11006), Alexa 488 goat anti-rabbit (A11034), Alexa 647 goat anti-guinea pig (A21450), and Alexa 647 donkey anti-rat (A78947).

Samples were blocked with 5% normal goat serum in PBS-T for ~60 mins at room temperature on a nutator. Thoraxes were incubated overnight in antibody on a nutator at 4°C, and then washed 3 times in PBS-T. Thoraxes were incubated overnight at 4° C in secondary antibody and Rhodamine-phalloidin or HRP. Probes stained with HRP 647 were incubated for two nights to increase staining penetration and signal. Samples were washed in PBS-T 2x for 5 mins, 2 x for 10 mins, and 1x for 30 mins. HRP 647 stains were washed and additional 30 mins.

Sample were mounted on slides with Vectashield containing DAPI (Biozol).

2.3.3 Confocal microscopy

Stained slides were analysed in the Core Facility Bioimaging at the LMU, Biomedical Center (Martinsried, DE) using a Leica SP8X WLL upright confocal microscope, equipped with an HCPL FLUOTAR 10×/0.30 objective for 10-fold magnification and a HCPL APO 63×/1.4 OIL CS2 objective for 63-fold magnification. The microscope was running with the Leica LAS X software. The obtained images were viewed and quantified using the ImageJ-software (FiJi). For measurement of the sarcomeres, the Myofibril-J plugin developed by Drs. Giovanni Cardone and Maria Spletter was used. Imaris was used to trace axon projections. Data were tabulated and recorded in Excel, and plotted and analysed in GraphPad Prism.

2.4 Biochemical procedures

2.4.1 Western blot

In this study 8 brains or 12 IFM were dissected from adult flies of the genotype of interest. Samples were homogenised in 20 µl of freshly made SDS-buffer (2% SDS, 240 mM Tris, pH 6.8, 0.005% bromophenol blue, 40% glycerol, and 5% βmercaptoethanol), incubated at 95°C for 3 min and stored at -20°C. Samples were run on 10% SDS-PAGE for separation and then transferred onto nitrocellulose membranes (Amersham Protran 0.2 µm NC) for 1 h at 120 V. Membranes were stained with Ponceau S (Sigma-Aldrich) to access the quality of the blotting. Membranes were de-stained and blocked with 5% non-fat milk solution in 0.5% Tween-TBS buffer (T-TBS) for 1 h and incubated for 1 h at room temperature with primary antibodies (guinea pig anti-Ime4, 1:1000; rabbit anti-H2AZ, 1:2,000; mouse anti-GFP, 1:1000). Membranes were washed three times with T-TBS for 15 min and incubated with goat anti-guinea pig HRP-conjugated secondary antibodies (Bio-Rad, 1:10000) for 1 h at room temperature. After three rounds of washes, the membranes were developed using Immobilion Western chemiluminescent (Milipore) substrate and exposed to X-ray films (Fuji medical X-ray, Super RX-N) or imaged on a ChemiDoc MP (Bio-Rad).

2.4.2 **Dot blot**

For the dot blot experiments in this study brains or IFMs from 8 wildtype or mutant flies were dissected. The obtained samples were homogenized in 10x Tri-Star/Trizol. 20% of the total solution volume of chloroform was added. The solution was then shaken for 15 seconds and kept at room temperature for 10 minutes. This step was followed by centrifuging the solution for 5 min to separate the phases. The upper aqueous phase, containing the RNA, was transferred to a new tube and 1-2 µl glycogen carrier was added.

For precipitation, isopropanol was added at a ratio of 1:1, and the new solution was kept again for 10 mins at room temperature. After that, the solution was centrifuged at 4° C for 10 mins. Centrifugation was followed by washing the RNA precipitate with 70% ethanol 2x and centrifuging at 4° C for 10 minutes. Once finished, the supernatant was removed and the RNA pellet was air dried. The pellet itself was subsequently dissolved in DEPC treated water, including incubation at 50°C if necessary to help dissolve the pellet. To remove genomic DNA, ~1-25 μ g of RNA samples were treated with 1 μ l of DNAse and 10 μ l of NEB-DNAse buffer, diluted with 100 μ l of water. This solution was kept for 10 minutes at 37° C. For heat inactivation, 5 mM EDTA were added to the solution and samples were kept for an additional 10 minutes at 75° C. Samples were then stored until further use at -80° C.

For dot blotting samples of 500 ng, 750 ng and 1000 ng were given into 5-10 µl RNAse free water. Those samples were then denatured for 10 minutes at 65° C and subsequently put on ice for 5 minutes. In the next step, an H-bond N+ Amersham membrane and a Whatman paper were wetted in 10 mM NaOH, 1 mM EDTA solution. The wetted Whatman paper was put on top of a dry piece of Whatman paper, and the wetted membrane was placed on top of the wetted paper. The prepared RNA samples were then spotted on the membrane and allowed to sink in. The membrane was crosslinked in a UV crosslinker at 120 mJ/cm² for ~ 1 min. The membrane was blocked in blocking solution for 1 hour at room temperature. The blocking solution consisted of 1x PBS, 0.02% Tween-20 and 5% non-fat-milk. The samples were then incubated with a rabbit anti-m6A antibody (Abcam) at 1:5000 dilution in the blocking solution at 4° C overnight. After incubation the samples were washed 3-6 times in a washing buffer consisting of 1xPBS and 0.02% Tween-20. The washing procedure was followed by a second incubation with an HRP conjugated goat anti rabbit antibody at 1:10000 dilution for 1 hour. After three rounds of washes as described above, the membranes were developed using Immobilion Western chemiluminescent (Milipore) substrate and exposed to X-ray films (Fuji medical X-ray, Super RX-N) or imaged on a ChemiDoc MP (Bio-Rad).

2.4.3 qPCR

For qPCR experiments, 200 IFM of adult flies were dissected as described [48]. Genotypes here were wildtype w^{1118} as control, mutant $Ime4^{\Delta 22-3}$ / Df(3R) Exel6197(III) and Mef2~Gal4~x~NIG~5339-R knockdown flies. RNA extraction was done as described in the dot blot method in 2.4.2. cDNA from those samples was prepared following the protocol of Luna Script RT Super Mix kit from New England Biolabs. Forward and reverse primers were designed to span introns and were ordered from MetaBion. Primers were diluted in water at 60°C to a concentration of 100 µmol.

For qPCR analysis, 1.5 µl primer solution, 6 µl cDNA and 7.5 µl SybrGreen were pipetted together. All wells to be analysed were then sealed with light-permissive plastic foil. The PCR plates were briefly centrifuged and remaining bubbles were removed by tapping. The prepared plates were finally placed in the QuantStudio3 qPCR machine, made by ThermoFisher. The machine was then set to its fast 7500 SybrGreen method and run on this programme. Obtained data was then transferred to Excel.

2.4.4 RT-PCR

For RT-PCR experiments, 200 IFM of adult flies were dissected as described [48]. Genotypes here were wildtype w^{1118} as control, mutant $Ime4^{\Delta 22-3}/Df(3R)$ Exel6197(III) and Mef2~Gal4~x~NIG~5339-R knockdown flies. RNA was extracted with Trizol as described in 2.4.2. cDNA was prepared with the Luna Script RT Super Mix kit (New England Biolabs). For the PCR reaction, 0.8 μ l Taq-polymerase, 2.5 μ l forward and 2.5 μ l reverse primer, 1 μ l cDNA and 1 μ l dNTP were diluted in 40 μ l water. 10x Taq buffer was added to a concentration of 5 μ mol. Samples were amplified on a c1000 touch PCR-machine (BioRad). The machine was set for 34 cycles at 58°C and 1 minute annealing time. The amplified products were then loaded a 1.5% agarose gel containing 0.2 % ethidium bromide at a ratio of 1:750. A 1 kb+ marker (Invitrogen) was finally added to the gel.

The prepared gel was transferred to an electrophoresis basin and wired to 100V for 35 minutes. After this time, the gel was transferred to GelDoc quantum (Vilber) for documentation.

2.4.5 Proteomics (Mass Spectrometry)

200 IFMs from each control w^{1118} , mutant Ime $4^{\Delta 22-3}$ / Df(3R) Exel6197(III), and rescue Mef2-Gal4/UAS-Ime4; Ime4^{∆22-3}/ Df(3R) Exel6197(III) flies were dissected as described above in 2.4.4, and then snap frozen on dry ice after removing buffer. IFMs were harvested from groups of 10 flies, and then after batch thawing on ice, IFMs from 50 flies were pooled per biological replicate, with in total 4 replicates per genotype. Samples were processed using the PreOmics iST Sample Preparation Kit (Preomics, #0000.0061) following the manufacturer's instructions. Prepared peptides were submitted to the Protein Analysis Unit (ZfP) at the LMU Biomedical Center. Desalted peptides were injected in an Ultimate 3000 RSLCnano system (Thermo) and separated in a 25-cm analytical column (75µm ID, 1.6µm C18, IonOpticks) with a 100-minute gradient from 5 to 60% acetonitrile in 0.1% formic acid. The effluent from the HPLC was directly electro sprayed into an LTQ Orbitrap XL (Thermo). Survey full scan MS spectra (from m/z 375–1600) were acquired with resolution R=60.000 at m/z 400 (AGC target of 3 x 10^6). The 10 most intense peptide ions with charge states between 2 and 5 were sequentially isolated to a target value of 1 x 10⁵, and fragmented at 27% normalized collision energy. Typical mass spectrometric conditions were: spray voltage, 1.5 kV; no sheath and auxiliary gas flow; heated capillary temperature, 250 °C; ion selection threshold, 33.000 counts. MaxQuant 1.6.14.0 (Cox et al., 2014)(159) was used to identify proteins and quantify by LFQ with the following parameters: Database, Uniprot AUP000000803 Dmelanogaster Isoforms 20210325.fasta; MS tol, 10 ppm; MS/MS tol, 20 ppm; Peptide FDR, 0.1; Protein FDR, 0.01 Min. peptide Length, 5; Variable modifications, Oxidation (M); Fixed modifications, Carbamidomethyl (C); Peptides for protein quantitation, razor and unique; Min. peptides, 1; Min. ratio count, 2. Additional analysis was performed in Perseus (160) (Tyanova and Cox, 2018).

To retain biologically relevant protein groups with "true negative" missing intensities between mutant and control samples (i.e., missing not at random, MNAR), we filtered the data by requiring at least three replicates in either group to contain a value, and we imputed missing values by replacement with a constant value (lowest observed intensity - 1). Differential expression was tested by t-test with FDR = 0.05. Results were exported and further analysis performed in R.

2.4.6 Transcriptomics (mRNA-Seq).

2 replicates of IFMs from 100 flies per genotype were dissected as previously described [48]. Genotypes included control w^{1118} , mutant $Ime4^{\Delta 22-3}/Df(3R)$ Exel6197(III), and rescue Mef2-Gal4/UAS-Ime4, $Ime4^{\Delta 22-3}/Df(3R)$ Exel6197(III). RNA was isolated with Trizol. Poly(A)+mRNA was purified using Dynabeads (#610.06, Invitrogen) and its integrity was subsequently verified on a Bioanalyzer (Agilent Technologies). The sequencing library was created with the library prep kit for Illumina (New England Biolabs) following the manufacturer protocol. Size selection was performed with SPRI select beads. For amplification of the obtained c-DNA samples, the oligonucleotides from Primerset 4 (NEB) of the kit were used. Amplification was then done by 7 PCR cycles. The quality of the library was verified once more with a Bioanalyzer (Agilent Technologies). Finally, sequencing was performed on an Illumina NextSeq at the LaFuga core facility of the LMU. Samples were sequenced as stranded, 150 bp paired-end to a depth of about 70 million reads.

Sequence data was mapped with STAR to ENSEMBL genome assembly BDGP6.22 (annotation dmel_r6.32 (FB2020_01)). Files were indexed with SAMtools and processed through featureCounts. Downstream analysis and visualization were performed in R using packages including DESeq2, DEXSeq, ggplot2, plyr, ComplexHeatmap, and viridis. Differential gene expression was analyzed with DESeq2, and differential exon use was determined with DEXSeq. Differentially expressed exons reflect both alternative splicing and alternative promoter use. Both packages were additionally used to generate normalized counts values. We employed previously annotated sets of genes, including sarcomere proteins (42) and all genes with the Flybase GO terms "muscle contraction," "actin cytoskeleton," "neuromuscular junction", or "synapse".

Plots were generated using ggplot2 or ComplexHeatmap. Unless otherwise stated, we used an adjusted p-value threshold of 0.05 for significance. If a log₂FoldChange threshold was used in a specific analysis, it is specified in the legend for the relevant figure panel.

2.5 Data processing

Obtained data was tabulated using Microsoft Excel. Sample numbers are stated, and were at least 10 individuals in all experiments. Statistical analysis and tests were performed with the GraphPad Prism software. For two-sample comparisons we used t-tests, and for experiments with three or more samples we used ANOVA with post-hoc Tukey tests of significance comparing all sample means. Images were initially processed in ImageJ (Fiji) as .tif files, and exported as .jpg for figures. Axonal tracing was done with Imaris. Figures and tables were created with Affinity Designer and Affinity Photo software.

3. Results

3.1 Behavioral assays

3.1.1 Flies lacking the Mettl3 methylase are flightless and exhibit motor deficits

In a candidate screen, we observed that muscle-specific RNAi against Mettl3 or Mettl14 driven by Mef2-Gal4 results in flightless flies [49], indicating that the m6A pathway may play an intrinsic role in muscle. With the aim of testing what role Mettl3 plays in *Drosophila* muscle, we generated trans-heterozygous mutants of Mettl3 $^{\Delta22-3}$ crossed to Df(3R) Exel6197, which spans the Mettl3 locus. Mettl3 $^{\Delta22-3}$ is a P-excision allele that deletes most of the coding region, including the catalytic domain [26] With the obtained transheterozygous mutant flies, we then performed a panel of behavioural tests. We found that the mutant flies were almost completely flightless compared to wildtype (Fig.1 A). Also, we saw, that the mutant flies exhibited strong defects in their ability to climb. Only around 15% of mutant flies were able to climb 5 cm in 3 seconds, whereas around 80% of wildtype flies could climb this distance (Fig.1 B). Finally, we observed held out wings in around 40% of the assayed mutant flies, but we could not see any matching phenotype within the wildtype control group (Fig.1 C). These data are consistent with previously reported Mettl3 phenotypes [22, 40], and demonstrate defects in the function of IFM, DFM, and leg muscles in flies lacking Mettl3.

3.1.2 Mettl3 is expressed and functionally active in both brain and IFM

Previous studies have focused on the role of Mettl3 in the fly nervous system and embryonic development [22, 26, 40, 50]. To demonstrate that Mettl3 is also expressed in IFM, we performed immunostaining and Western blot. Using immuno-fluorescence and confocal imaging, we observed Mettl3 expression in adult IFMs (Fig. 1 D-1 – D-3) that was absent in $Mettl3^{\Delta 22-3} / Df(3R)$ Exel6197 (Fig. 1 E-1 – E-3).

Interestingly, this Mettl3 signal was both nuclear and cytosolic. Mettl3 was also clearly detected by Western blot in both in dissected brain and IFM tissue from w^{1118} control flies, and this band was lost in $Mettl3^{\Delta 22-3}$ / Df(3R) Exel6197 tissues (Fig. 2 C). All together these experiments indicate that Mettl3 is expressed in both neurons and IFM, and also demonstrate that our mutant genotype is effective.

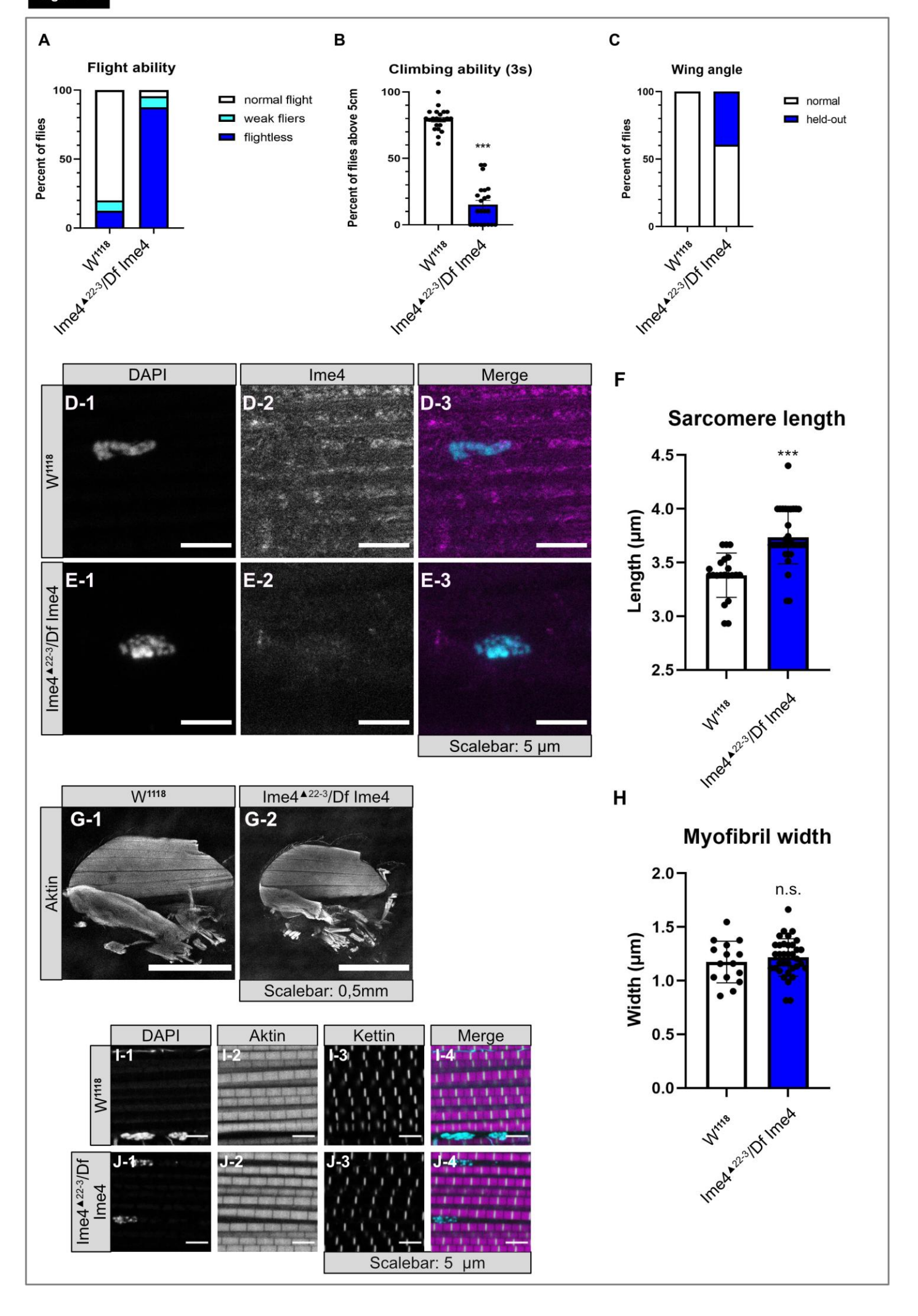
Mettl3 is the main methylase of the m6A pathway [40]. To test if it is functionally active in both muscle and neurons, we performed dot blots with an antibody that recognizes N6-methyladenosine. We could detect m6A marks on total RNA in both brain and IFM dissected from w^{1118} control flies (Fig. 2 A). $Mettl3^{\Delta 22-3} / Df(3R)$ Exel6197 flies are missing the main methylase Mettl3 and thus are expected to have a significant decrease of the m6A-mark in their RNA. Indeed, in neuronal as well as in muscle tissue we observed a significant decrease of m6A marks compared to the wildtype control flies (Fig. 2 A, B). This demonstrates that m6A methylation of RNA occurs in both brain, and presumably motor neurons, as well as in IFM.

3.1.3 Mutant sarcomeres are longer than in wildtype

To further understand why Mettl3 mutant flies are flightless, we analysed the myofiber and sarcomere structure of the mutant. IFM myofibers at 10x magnification looked normal spanning from anterior to posterior of the thorax in six bundles, and we saw no difference between the wildtype control and the mutant (Fig. 1 G-1 and G-2). However, at 63x magnification we observed mild defects and the mutant sarcomeres were different from the wildtype ones. Here we saw significantly longer sarcomeres of ~3.7 μ m in $Mettl3^{\Delta 22-3}$ / Df(3R) Exel6197 flies compared to ~3.4 μ m in wildtype w^{1118} (Fig. 1 I-2, I-3, J-2, J-3, F). However, Kettin was still correctly localized to the z-disc and z-disc structure was intact (Fig. 1 I-3, J-3). Myofibril width was also unaffected (Fig. 1 H). Sarcomere length in IFM is tightly regulated, and the observed increase in length would likely disrupt IFM contractility.

Figure 1. Mettl3 is expressed and regulates sarcomere length in Drosophila IFM.

- (A-C) Plots quantifying behavioural defects in Mettl3 mutant flies in their ability to fly (A) (flightless, dark blue; weak fliers, light blue; normal flight ability, white), their ability to climb (B) (control, white; $Mettl3^{\Delta 22-3}/Df$ mutant, blue) and their tendency to hold out their wings (C) (normal wing position, white; held-out wing position, blue). For those Experiments over 100 male flies were tested each on a time course of several days. Mutant flies were obtained from several independent crosses. (D-E) Single-plane confocal images of wildtype (D1-3) and $Mettl3^{\Delta 22-3}/Df$ mutant (E1-3) IFMs stained with antibodies against Mettl3. Mettl3 is detected both in the nucleus and cytoplasm and is not detected in the trans-heterozygous mutant. Scale bar = 5 µm. DAPI, cyan; Mettl3/Ime4, magenta. For those experiments 7 thoraxes were imaged each.
- **(F)** Quantification of sarcomere length of the data shown in I-1 to J-4. Significance determined by t-test, n.s. = not significant; ***, p-value < 0.001.
- (G) Confocal z-projections of wildtype and mutant IFM myofibers at 10x magnification. Myofibers are intact and grossly normal. Scalebar = $500 \mu m$. phalloidin stained actin, grey. 5 thoraxes were imaged each.
- **(H)** Quantification of myofibril width of the data shown in I-1 to J-4. Significance determined by t-test, n.s. = not significant; ***, p-value < 0.001.
- (I-J) Single-plane confocal images of wildtype control w^{1118} (H1-4) and $MettI3^{\Delta 22-3}/Df$ mutant (I1-4) IFM myofibrils. Although the sarcomere structure is intact, mutant sarcomeres are too long. Scalebar = 5 µm. DAPI stained nuclei, cyan; phalloidin labelled actin, magenta; Kettin-labelled z-discs, yellow. 5 thoraxes were imaged each.



3.1.4 Tissue-selective knockdown of Mettl3 using RNAi in muscle or neurons

Previous studies have suggested that flight defects in *Mettl3* mutant flies can be attributed to neuronal deficits [50]. However, our data revealed a structural defect in IFM sarcomeres, and we hypothesized this may be due to muscle-intrinsic Mettl3 function. To test if this is due to Mettl3 function in muscle or neurons, we used tissue-specific RNA interference (RNAi) mediated by the UAS-Gal4 System. We selected Mef2-Gal4, which is expressed selectively in muscle tissue [51], and Elav-Gal4, which is expressed specifically in neurons, including motor neurons [52]. To find the most effective RNAi lines, we screened all available lines targeting Mettl3 itself, its stabilising protein Mettl14, and the YTH-reader proteins. We selected the hairpin that generated the strongest and most consistent flightless phenotype for further analysis (Fig. 3). This hairpin was obtained from the NIG-fly stock center in Japan and had the stock number 5339-R, and will be referred to as Mettl3-IR^{NIG-5339}.

We performed a Western blot for Mettl3 to check if the UAS-Gal4 system would in fact knock down tissue specifically. In the Western blot, we could detect Mettl3 in wildtype w^{1118} brain and IFM, as well as in control samples when the drivers alone were crossed to the wildtype (Fig. 2 C). By contrast, we saw significant decreases in Mettl3 protein expression as compared to the control when Mettl3-IR^{NIG-5339} was crossed to either Elav-Gal4 or Mef2-Gal4. We saw the same effect with Mettl3-IR^{BL80431} crossed Mef2 Gal4. Importantly, with Mef2-Gal4 crosses we lost the Mettl3 band in muscle tissue but not in brain, while with Elav-Gal4 crosses we lost the Mettl3 band in brain (Fig. 2 C). This indicates that we can effectively knockdown Mettl3 using RNAi in a tissue-specific manner.

Furthermore, we investigated the specificity of the NIG-5339 hairpin itself. To do this, we rescued the phenotype caused by this hairpin by overexpression of Mettl3 using a UAS-Mettl3 [53]. The experimental flies had the NIG-5339 hairpin driven in muscle by Mef2-Gal4, but we added back another UAS-cassette containing a functional copy of Mettl3. Approximately 20% of *Mettl3-IR*^{NIG-5339} die in the pupal case, and while lethality was significantly reduced to only 10% of *Mettl3-IR*^{NIG-5339}, *UAS-Mettl3* pupa (Fig. 4 I).

We saw a similar effect with jumping ability, where *Mettl3-IR*^{NIG-5339} flies jump significantly shorter distances than control *Mef2-Gal4* x *w*¹¹¹⁸ flies. The jumping ability significantly increased once Ime4 was overexpressed in *Mettl3-IR*^{NIG-5339}, *UAS-Mettl3* as compared to the muscle knockdown (Fig. 4 J). We were unable to rescue the flight phenotype, potentially indicating differences in Mettl3 function in fibrillar IFM required for flight versus tubular leg and jump muscles required for jumping and eclosion. Taken together these experiments indicate that our Mettl3 knockdown was specific.

Figure 2. Validation of mutant, RNAi, and overexpression tools reveals that Mettl3 and the m6A mark are present in both brains and IFM.

- (A) Dot-blot image of both brains and IFM dissected from control w^{1118} and $Mett/3^{\Delta 22-3}/Df$ mutant flies. Anti-m6A antibodies were used to detect the mark in increasing amounts of total RNA ranging from 0.5 µg to 2 µg. The mutant rows show decreased signal intensities as compared to the control. For this experiment 8 IFMs of wildtype and mutant were analysed for 4 different concentrations. This experiment was carried out on 3 times on different days.
- **(B)** Semi-quantitative analysis of the fold-change in dot blot intensities from (A). Data from three independent experiments were combined in the plot. w^{1118} (white) and $Mettl3^{\Delta22-3}/Df$ (blue), significance determined by t-test, n.s. = not significant; ***, p-value < 0.001.
- **(C)** Western blots, stained with antibodies against Ime4/Mettl3 with anti-H2AZ used as a loading control. Ime4/Mettl3 protein is not detected in brain or IFM dissected from $Mettl3^{\Delta 22-3}/Df$ mutant flies, but can be detected in both IFM and brain dissected from control w^{1118} . Ime4 can be knocked down tissue specifically using RNAi hairpins targeting Ime4 and a tissue specific Gal4 driver. Mef2-Gal4 is expressed in muscle, while Elav-Gal4 is expressed in neurons. NIG hairpin 5399-R and Bloomington hairpin Bl8043 both target Mettl3. This data was obtained from 8 brains and 12 IFMs both of wildtype and mutant. This experiment was carried out on 4 times on different days.
- **(D)** Western blot stained as in (C). Mettl3 can be rescued tissue-specifically by expressing in in a target tissue (D). In Mef2-Gal4 rescues, Mettl3 is detected in IFMs but only weakly in brain. In Elav-Gal4 rescues, Mettl3 is detected in dissected brains but only weakly in IFMs. H2AZ was used as a loading control. This data was obtained from 8 brains and 12 IFMs both of wildtype and mutant. This experiment was carried out on 3 times on different days.
- **(E-F)** Semi-quantitative analysis of the western blots for the tissue specific knockdown (C) and the rescue (D). Quantification shows strongly reduced expression in control tissues from $Mettl3^{\Delta 22}$ - $^{3}/Df$ (blue), and tissue-specificity of knockdown (E) or rescue (F) with Mef2-Gal4 (red) or Elav-Gal4

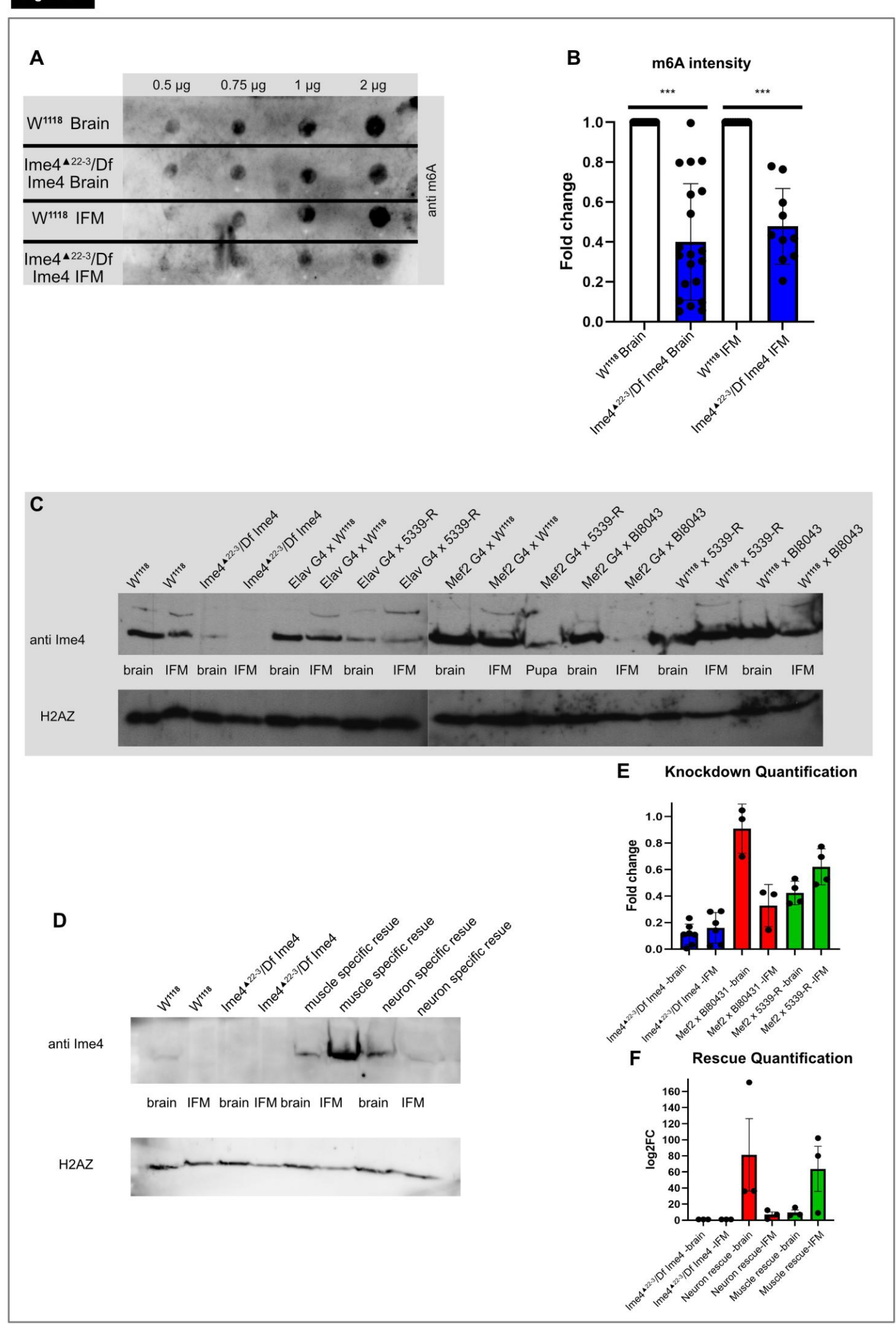
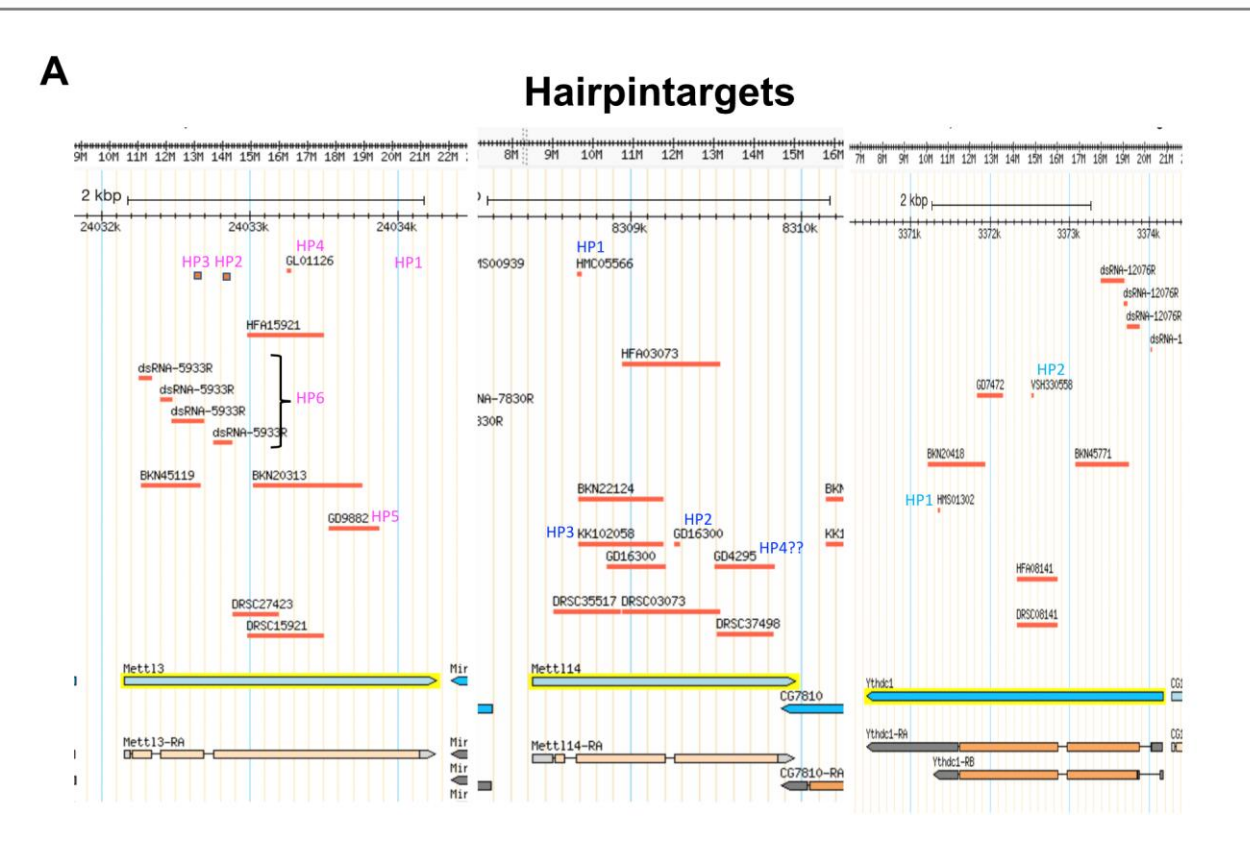
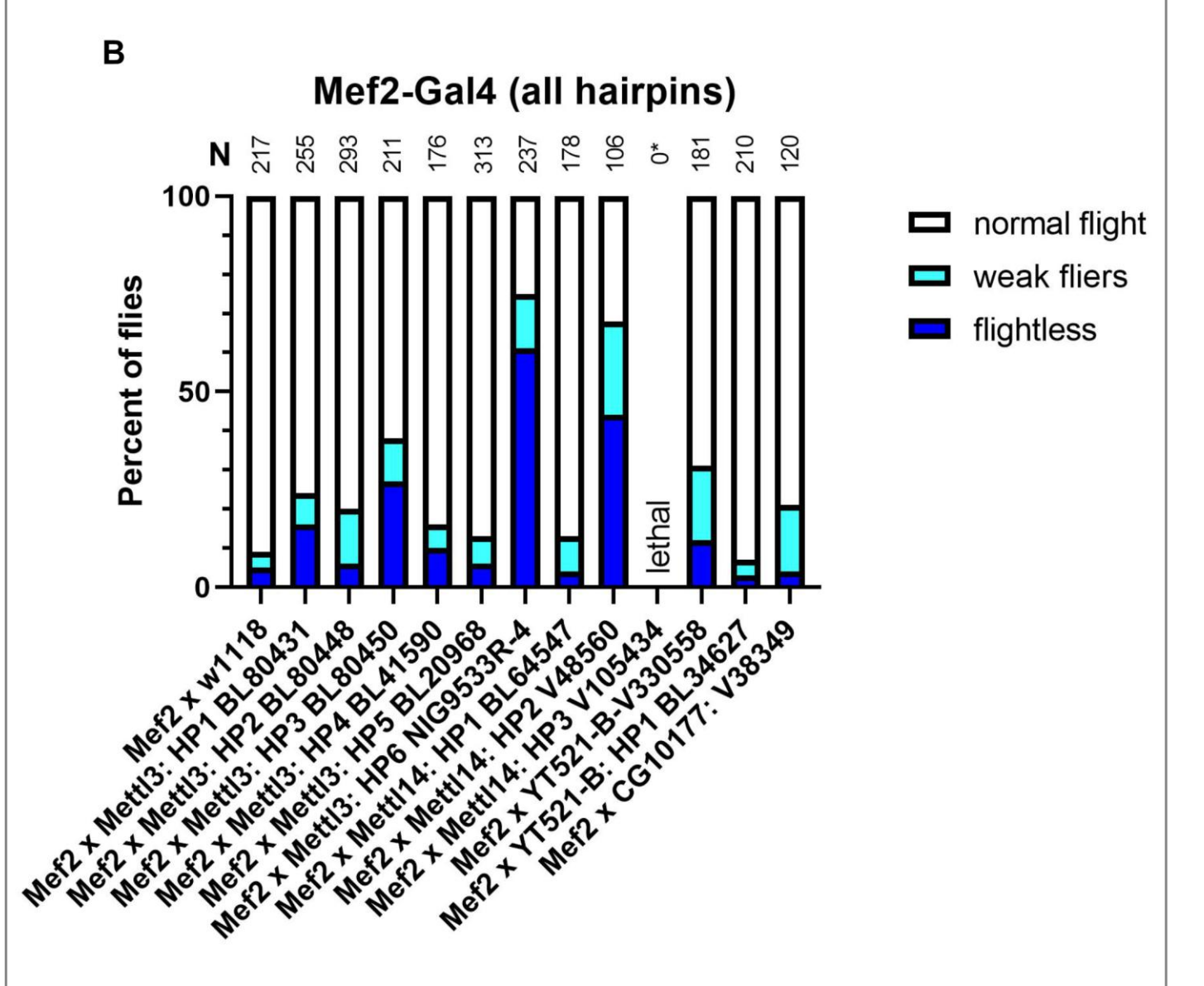


Figure 3. Screen identifies RNAi hairpins targeting Mettl3 and Mettl14 that both cause flightless phenotypes.

- **(A)** Flybase screenshots showing the sequences targeted by all hairpins used to knockdown three genes of interest in the Mettl3 pathway used in this experiment (Mettl3, Mettl14 and Ythdc1). Mettl3 has m6A enzymatic activity, Mettl14 is an essential co-factor in the writer complex, and Ythdc1 is an m6A reader protein. The position of the hairpins relative to the target genes is marked.
- **(B)** Plot showing the flight ability of RNAi knockdown flies with different RNAi hairpins. Hairpin 6 (HP6, NIG 9533-R) was identified as the strongest RNAi hairpin targeting *Mettl3*, and is used in subsequent experiments. For Mettl14, we identified V105434 from the Vienna stock center as the strongest hairpin resulting in lethality, while V48560 produced a strong flightless phenotype. Hairpins against Ythdc1 were either not effective, or Ythdc1 is not required in IFM, as we did not observe a strong flight phenotype. Together, independent hairpins targeting multiple components of the Mettl3 pathway identify a muscle-specific function of Mettl3 required for normal flight ability. N = total number of flies tested.





3.1.5 Muscle-specific Mettl3 knockdown results in flightlessness

Having validated our RNAi reagents and tissue-specific drivers, we performed a panel of behavioural tests to determine which behaviours are dependent on Mettl3 function in muscle versus neurons. We saw a strong flightless phenotype in the muscle specific knockdown when the NIG-5339 hairpin was crossed to the Mef2-Gal4 driver. Around 60% of the tested flies were flightless and another ~15% were weak fliers (Fig. 4A). However, when we crossed the hairpin to the Elav-Gal4 driver combined with UAS-Dicer2 to enhance the neuronal specific Mettl3 knockdown, we only saw 20% flightless flies and around 50% weak fliers (Fig. 4 A). This indicates that in IFM both neurons and muscle contribute to the flightless phenotype, with the Mettl3 activity in the muscle itself playing a large role in the flight defect.

We next examined climbing ability. In the muscle-specific Mettl3 knockdown with Mef2-Gal4, we did not see a distinguishable phenotype: their climbing ability was not significantly different from the control (Fig. 4B). By comparison, in the neuronal specific knockdown we saw a strong climbing phenotype that was comparable in severity to that of $Mettl3^{\Delta 22-3} / Df(3R)$ Exel6197 (Fig. 4 B). We interpret this to mean that neuronal deficits, rather than muscle deficits, are responsible for the climbing phenotype. Held-out wings were observed with both muscle and neuronal-specific knockdown, but $Mettl3^{\Delta 22-3} / Df(3R)$ Exel6197 animals had a much strong held-out wing phenotype (Fig. 4 C).

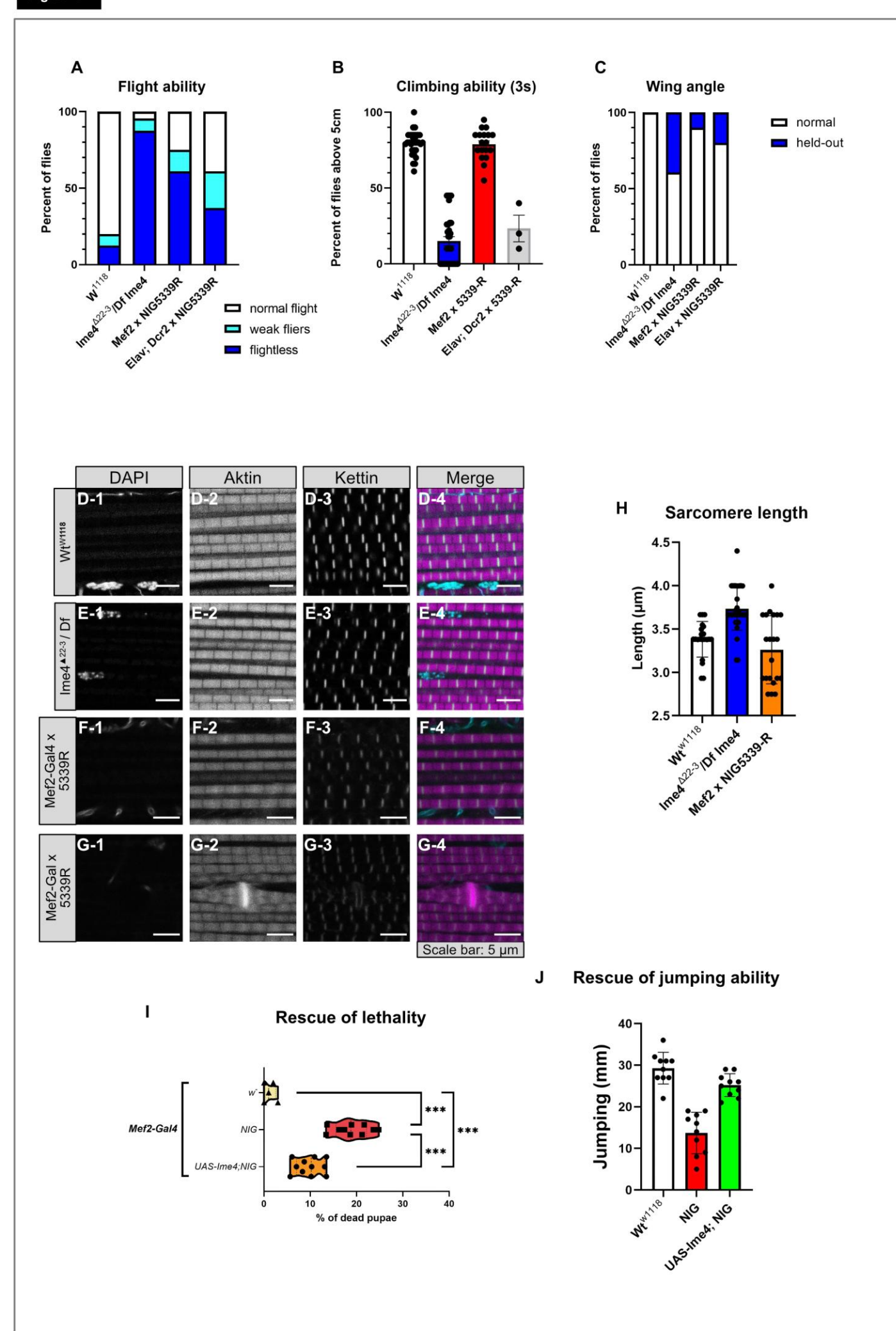
3.1.6 Sarcomeres in muscle-specific knockdown IFM show defects

We next examined sarcomere structure in Mef2-Gal4 driven *Mettl3-IR*^{N/G-5339} flies. We expected that if Mettl3 plays an intrinsic role in IFM, we should observe a sarcomere defect like we observed in $Mettl3^{\Delta 22-3}$ / Df(3R) Exel6197 flies (Fig. 1 I-1 – J-4). In the muscle knockdown, we observed changes in sarcomere structure. Although myofibrils with regular sarcomeres formed, the length of the sarcomeres was variable as compared to the control (Fig. 4 D-1 – F-4, H). Here the sarcomeres were not uniformly longer, but instead we also saw sarcomeres which were even shorter or longer than wildtype.

Short sarcomeres may indicate hypercontraction [46], and the efficiency of knockdown in different flies could results in the observed variability in sarcomere length. We also saw overgrown Z-disk areas, known as zebra bodies, distributed irregularly in the IFMs in the muscle-specific knockdown (Fig. 4 G-1 – G4), which is indicative of hypercontraction or z-disc instability. We conclude that sarcomere defects observed in IFMs of $Mettl3^{\Delta 22-3}$ / Df(3R) Exel6197 and Mef2-Gal4 > Mettl3- $IR^{NIG-5339}$ are the result of muscle-intrinsic function of Mettl3.

Figure 4. Tissue specific RNAi knockdown supports a requirement for Mettl3 in both muscles and neurons.

- (A-C) Plots quantifying behavioural defects in Mettl3 mutant flies and Mettl3 tissue-specific RNAi knockdown flies in their ability to fly (A), their ability to climb (B) and their tendency to hold out their wings (C). Mef2-Gal4 driving in muscle results in impaired ability to fly, while Elav-Gal4 driving in neurons impairs both flight and climbing. Dcr2 enhances knockdown efficiency. Flight ability was assayed from over 100 male flies each from several crosses. Climbing ability and wing angle were assayed from 60 male flies each, also from several crosses.
- **(D-G)** Single-plane confocal images of wildtype control w^{1118} (D1-4), $MettI3^{\Delta 22-3}/Df$ mutant (E1-4) and Mef2-Gal4 x 5339R knockdown (F1-4, G1-4) IFM myofibrils. The sarcomere structure is intact but mutant and knockdown sarcomeres show defects in sarcomere length. The formation of zebra bodies (actin inclusions at the z-disc) (G1-4) is also prevalent in muscle specific knockdowns. Scalebar = 5 μ m. DAPI stained nuclei, cyan; phalloidin labelled actin, magenta; Kettin-labelled z-discs, yellow. 5 thoraxes were imaged each.
- **(H)** Quantification of sarcomere length of the data shown in D-1 to G-4.
- (I-J) Plots quantifying the percentage of dead pupae (I) and the jumping ability (J) in *w*¹¹¹⁸, Mef2-Gal4 x 5339R knockdown and flies with an UAS-Ime4 rescue construct. Lethality is significantly reduced and jumping ability increased as soon as Ime4 is overexpressed in the knockdown, indicating the specificity of the hairpin. Significance determined by ANOVA with posthoc Tukey, p-value < 0.001, ***). Lethality data was assayed from 5 wildtype replicates, 10 Mef2-Gal4 x 5339R replicates, and 11 UAS-Ime4 rescue constructs. Jumping data was obtained from 10 male flies per genotype. This experiment was conducted twice.



3.1.7 Tissue-specific expression of Mettl3 is unable to rescue mutant behavioural phenotypes

To test if Mettl3 indeed has a tissue-intrinsic function in muscle, we performed muscle-specific rescue of Mettl3 mutants. We made use of the Gal4-UAS system to express specifically in muscles with Mef2-Gal4 or neurons with Elav-Gal4 in a mutant background. One fly line we built had the tissue specific driver on the second chromosome and *Mettl3*^{Δ22-3} on the third: *Mef2-Gal4 / Cyo; Mettl3*^{Δ22-3} / *TM3, Ser.* The other fly line had a UAS-Mettl3 cassette on the second and *Df(3R) Exel6197* on the third chromosome: *UAS-Ime4 / Cyo; Df(3R) Exel6197 / TM3, Ser.* When those two lines were crossed together, we obtained mutant progeny which still could express working Mettl3 in muscles or neurons. (Fig. 5) We validated that our UAS constructs were expressed in a tissue-specific manner using Western blot. While the Mettl3 band is absent in IFM and brain dissected from mutant flies, Mef-Gal4 rescue flies express Mettl3 in IFMs and Elav-Gal4 rescue flies expression Mettl3 in neurons (Fig. 2 D).

This experiment therefore indicates that our rescue construct is working and Mettl3 is expressed tissue-specifically.

We next performed the same behavioural assays with the rescue flies that we had tested with the $Mettl3^{\Delta 22-3}$ / Df(3R) Exel6197 mutant and the $Mettl3-IR^{NIG-5339}$ knockdown flies. At room temperature, control w^{1118} flies were able to fly, and ~90% of mutant and control flies were flightless (Fig. 6 A). We thus do not see background noise or leaky expression of the Gal4-UAS system under our conditions. Neither the neuronal nor the muscle rescue could rescue flight ability (Fig. 6 A). The neuronal rescue performed best with ~70% flightless or weak fliers. These data suggest that Mettl3 may be required in both muscle and neurons to enable flight.

We were additionally unable to rescue climbing or held-out wing phenotypes by expression of Mettl3 in selectively muscle or neurons. In our climbing assays, only ~15% of mutant flies made it over the 5 cm line in 3 seconds. In the control groups (just the cassette or just a driver) as well as the Mef2-Gal4 and Elav-Gal4 rescue flies, only ~20-35% of flies were able to climb 5 cm in 3 seconds, and thus the rescue did not perform significantly better than the control groups (Fig. 6 B).

The rescue flies also did not differ significantly from controls and the mutant in the percent of flies with held-out wings (Fig. 6 C). In summary, at room temperature the Mettl3 phenotypes in flight, climbing, and wing positioning could not be rescued tissue specifically.

To increase the level of Mettl3 expression, we repeated the behaviour experiments after raising the rescue flies at 27° C. At this temperature, we saw a much better rescue with approximately 50% of flies able to fly with both Mef2-Gal4 and Elav-Gal4 rescue (supplementary Fig. 13). However, we also observed that the control group with UAS-Mettl3 and lacking a specific driver was also performing better with around 40 % able to fly, but the control group containing only the Gal4 driver performed comparable to the mutant genotype. This suggests that at 27° C the UAS-cassette gets leaky and hence its expression is not strictly limited to one tissue any more. Nevertheless, these results suggest that the flight phenotype can be rescued when Mettl3 expression is not limited to only muscular or neuronal tissue, but will be expressed in both instead.

This observation supports our hypothesis that the mutant phenotype is in fact coming from a neuronal and a muscular side.

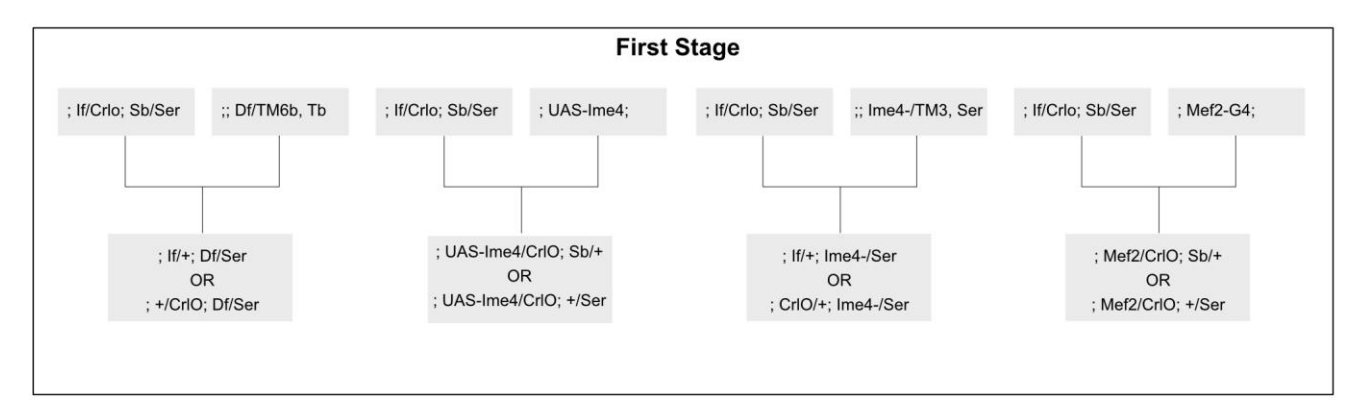
3.1.8 Muscle-specific Mettl3 expression can rescue the sarcomere phenotype

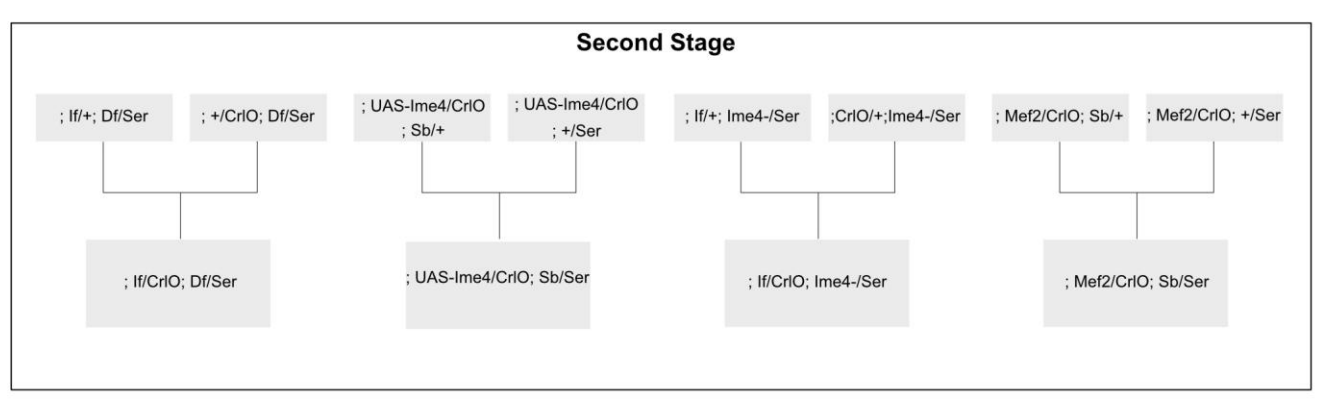
Our RNAi data showed that Mettl3 has an intrinsic function in muscle to regulate sarcomere length (Fig. 4 F-1 – F-4, G-1 – G-4, H). We reasoned that even if flight ability was not restored, our muscle-specific rescue might restore normal sarcomere structure. To text this, we imaged the sarcomere structure of our Mef2-Gal4 rescue flies and all the matching controls. We found that $Mettl3^{\Delta 22-3}$ / Df(3R) Exel6197 mutants as well as controls including just the UAS-cassette (UAS-Mettl3 / +; $Mettl3^{\Delta 22-3}$ / Df(3R) Exel6197) or just one of the two Gal4 drivers (Mef2-Gal4 or Elav-Gal4/+; $Mettl3^{\Delta 22-3}$ / Df(3R) Exel6197) had a sarcomere length of about 3.7 µm (Fig. 6 G). Sarcomeres in IFM from the neuronal specific rescue (Elav-Gal4/UAS-Mettl3; $Mettl3^{\Delta 22-3}$ / Df(3R) Exel6197) were also about 3.7 µm long and not significantly different from the mutant (Fig. 6 G).

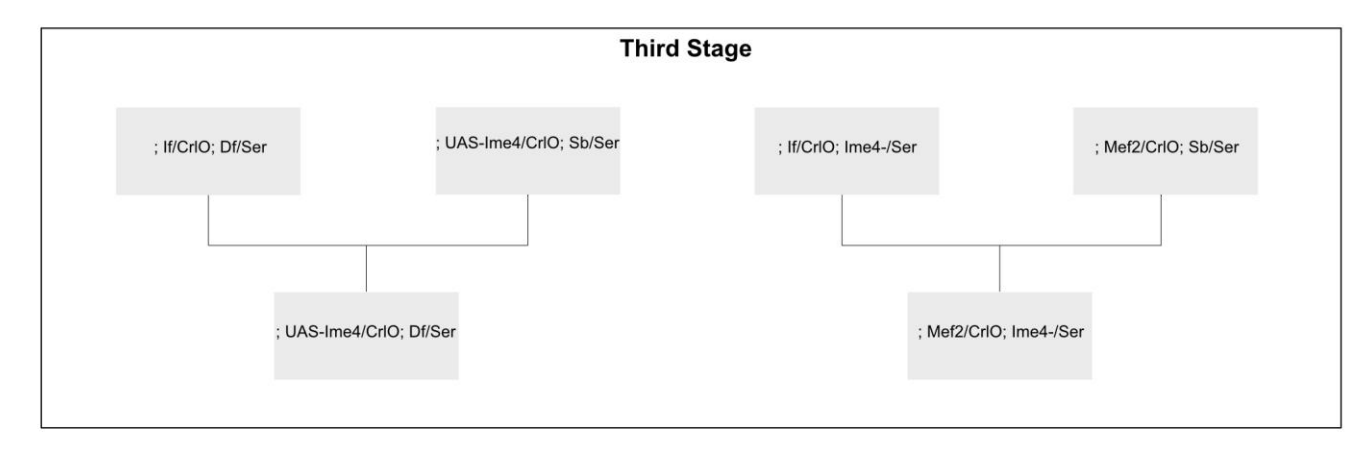
Remarkably, the muscle-specific rescue (Mef2-Gal4 / UAS-Mettl3; $Mettl3^{\Delta 22-3}$ / Df(3R) Exel6197) had an average sarcomere length of ~3.4 µm, and was therefore much closer to the wildtype control in length (Fig. 6 D-1 - F-4, G). This data suggests that muscle-specific expression of Mettl3 is sufficient to rescue the defects in sarcomere length in Mettl3 mutants, demonstrating a muscle-intrinsic function for Mettl3.

Fig. 5 Crossing scheme used to obtain tissue-specific Mettl3 rescue genotypes.

Crossing scheme illustrating how all four genetic elements were combined into a single fly to obtain the rescue genotypes. In the first and second stage of the scheme (top two boxes), the Mettl3 mutant chromosome ($Mettl3^{\Delta 22-3}$), the Mettl3 deficiency (Df) (Df(3R) Exel6197(III)), the UAS-Mettl3 construct ($UAS-Mettl3-HA^{attlP40}/CyO$) and a Gal4 driver (Mef2-Gal4/CyO) are double balanced. This has to be done in two steps to generate stably balanced fly lines. The second chromosome was balanced over CyO, while the third was balanced over TM3, Ser (Ser). In the third stage, one mutant copy of Mettl3 and one element of the UAS/Gal4 system are combined in the same fly. Since the full mutant genotype is sterile, the flies must be heterozygous for the Mettl3 mutation to be maintained as a stock. In the last stage (bottom) which generates the rescue fly (genotype in bold at the bottom, $Mef2-Gal4/UAS-Mettl3-HA^{attP40}$; $Mettl3^{\Delta 22-3}/Df(3R)$ Exel6197(III)), all genetic components are brought together generating an experimental fly that is homozygous mutant for Mettl3 with a UAS-Mettl3 expressed in a tissue determined by the tissue specific Gal4 driver. This scheme is an example, as instead of Mef2-Gal4 (Mef2), other drivers could also be used as long as they are on the same chromosome (Chromosome II). Df = Df(3R) Exel6197(III); $Ime4- = Mettl3^{\Delta 22-3}$; $Ime4- = Mettl3^{\Delta 22-3}$; Ime4-







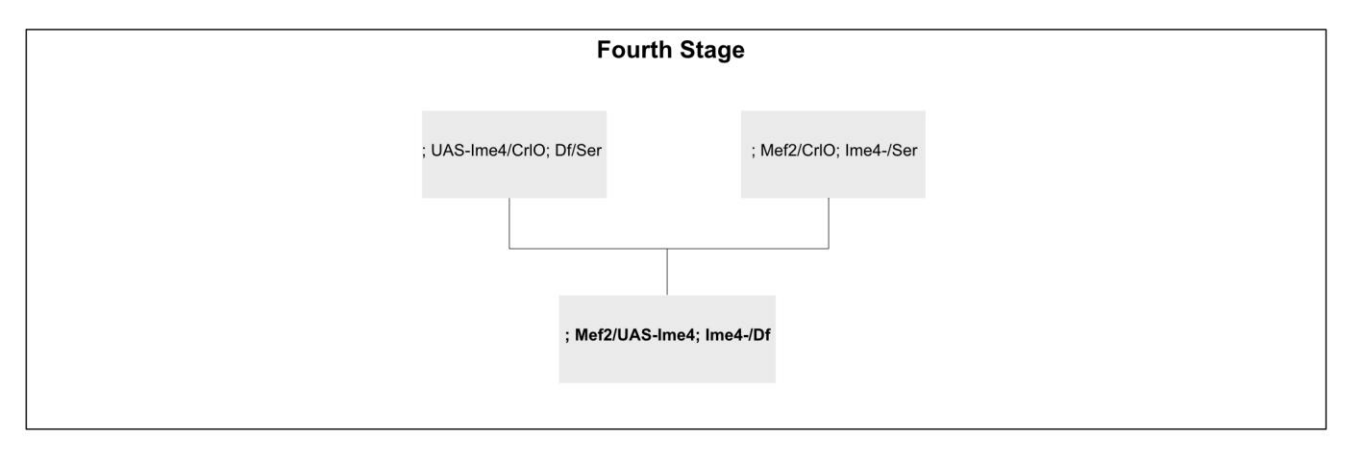
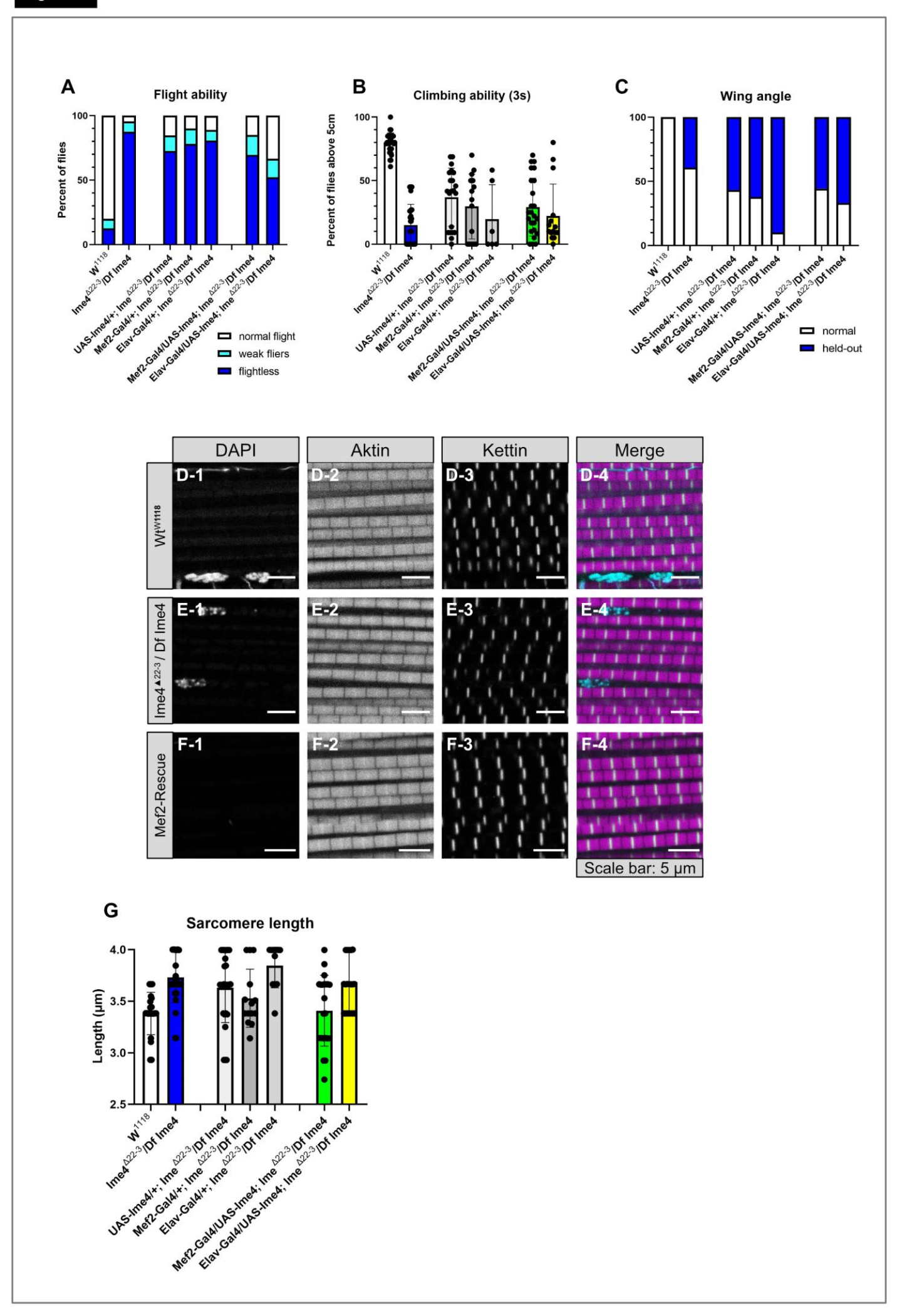


Figure 6. Tissue specific rescue can restore the sarcomere structure but not higher functions like flight, climbing, and wing posture.

- (A-C) Plots quantifying behavioural defects in Mettl3 mutant, control, and tissue-specific rescue flies in their ability to fly (A), their ability to climb (B), and their tendency to hold out their wings (C). Mef2-Gal4 drives in muscle, while Elav-Gal4 drives in neurons. Flight ability was assayed from over 100 male flies each from several crosses. Climbing ability and wing angle were assayed from over 60 male flies each, also from several crosses.
- **(D-F)** Single-plane confocal images of wildtype control w^{1118} (D1-4), $Mettl3^{\Delta 22-3}/Df$ mutant (E1-4), and muscle specific rescue (F1-4) IFM myofibrils. Mutant sarcomeres are too long, whereas wildtype and muscle specific rescue sarcomeres are indistinguishable. Scalebar = 5 μ m. DAPI stained nuclei, cyan; phalloidin labelled actin, magenta; Kettin-labelled z-discs, yellow. 5 thoraxes were imaged each.
- **(G)** Quantification of sarcomere length of the data shown in D-1 to F-4. Mef2-Gal4 (green) but not Elav-Gal4 (yellow) is able to rescue the sarcomere length defect.



3.1.9 Sarcomere proteins are misregulated in Mettl3 RNAi IFM

Having demonstrated that Mettl3 plays a role in *Drosophila* IFM in sarcomere development, we next investigated how loss of Mettl3 affects the expression of sarcomere proteins. To test the expression levels of certain muscle related proteins, we made use of GFP-tagged Fosmid reporter lines. Fosmid reporter lines contain a genomic fragment with a third copy of a C-terminally GFP tagged gene of interest inserted into attP-VK33 [54]. The inserted GFP-tagged genes are under the control of native regulatory elements, similar to genomic rescue constructs. The reporter lines were recombined with Mef2-Gal4, and then crossed to w^{1118} as a control and Mettl3- $IR^{NIG-5339}$ to knock-down Mettl3 expression. The obtained progeny were then imaged with the same confocal settings to quantitatively compare GFP fluorescence intensities.

We examined several proteins including Flightin (Fln), Myofilin (Mf), Obscurin (Unc-89), and Actin88F which are localized to different parts of the sarcomere [1]. Fln and Mf both localize to the thick filaments, and were significantly decreased in the knockdown background (Fig. 7 C-1 – F-4, M, N). The mean GFP intensity level of Fln-GFP in control was ~55 (mean brightness value) (Fig. 7 M), while in the knockdown background was only ~20 (Fig. 7 M), a fold change of 2.75. Mf-GFP intensity averaged ~60 in control, but was significantly decreased to ~15 in the RNAi (Fig. 7 E-1 - F-4, N), a 4-fold change. Unc-89 sits at the sarcomere M-line. In control, Unc-89-GFP had a mean GFP intensity around ~25, while in the knockdown this dropped significantly to ~9 (Fig. 7 G-1 - H-4, O), a fold change of 2.8. This decrease in expression appears to affect not only specific sarcomere proteins, as Act88F, which forms the thin filaments, displayed also a significant decrease between the wildtype control and the RNAi knockdown (Fig. 7 A-1 - B-4, K). This suggests that Mettl3 normally regulates the expression of select sarcomere proteins.

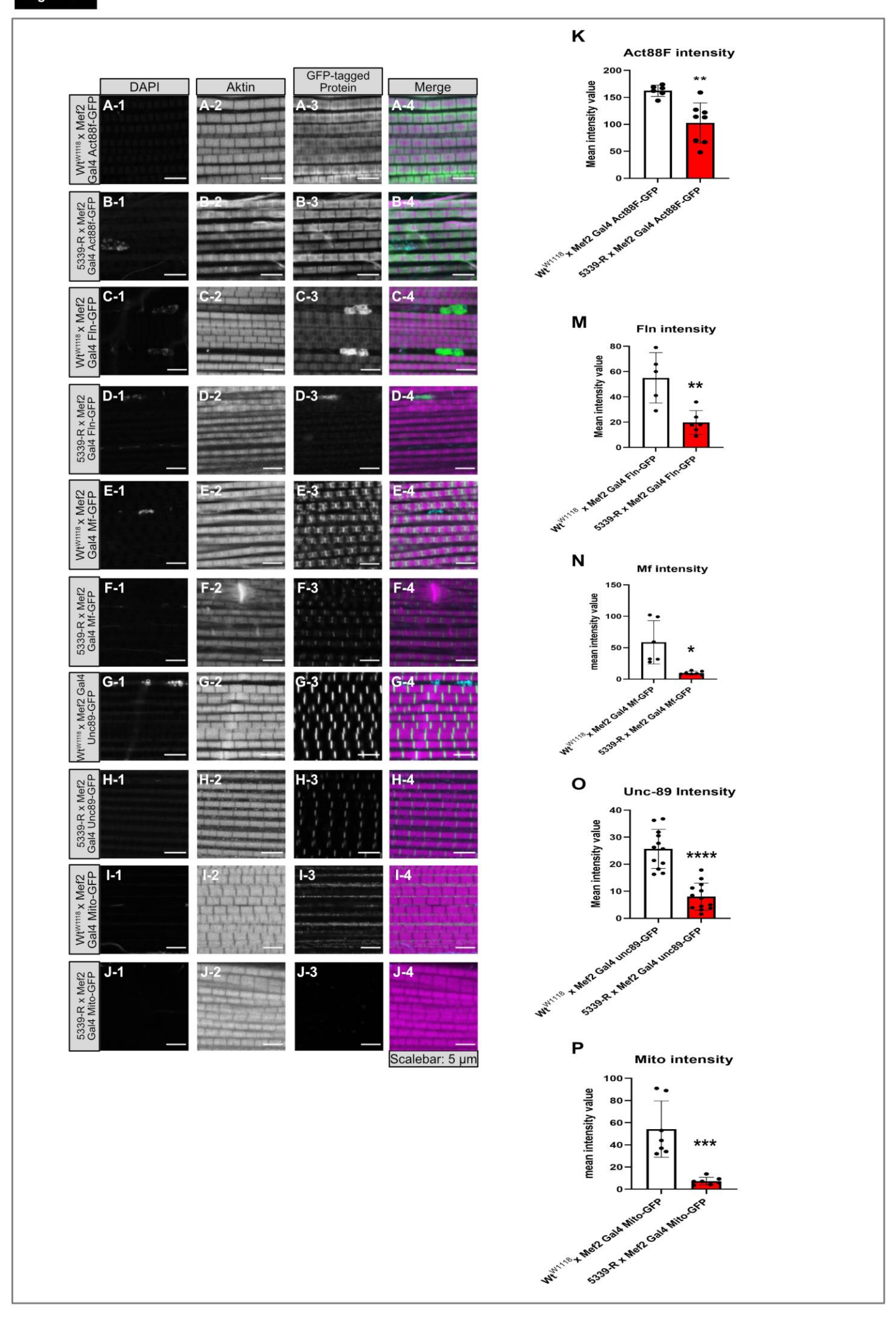
3.1.10 Expression of UAS-mito-GFP shows a strong decrease in muscle specific Mettl3 knockdown

In addition to sarcomere components, we were interested in potential differences in mitochondria that might contribute to sarcomere or functional defects in IFM. Normally the mitochondria within the IFM in Drosophila will fuse during development [55]. It is proposed that mitochondria form long, string-shaped patterns between the myofibrils and spanning alongside them to cope with the strong energy demand of IFM tissue. To explore the mitochondria, we made use of a UAS-mito-GFP reporter line, which is a GFP-tagged version of the enzyme Cox8A, which is located in complex IV within the mitochondria [56]. In the control, the mitochondrial signal was located in strings or an elongated network structure alongside the myofibrils (Fig. 7 I-3). In the *Mettl3-IR*^{N/G-5339} knockdown however, the signal was significantly reduced (Fig. 7 J-3, P) and the mitochondrial network was much less elaborate. The mean brightness intensity of the control was ~55, whereas in the knockdown was around ~7. Thus, we see a 7.8-fold decrease in mitochondrial signal upon Mettl3 knockdown, suggesting that mitochondrial associated genes are also affected.

Figure 7. Expression of multiple sarcomere proteins is decreased in Mettl3 knockdown flies.

(A-J) Single-plane confocal images of GFP-tagged reporter expression in IFM for GFP-tagged Fosmid including Act88F (B1-4), Fln (D1-4), Mf (F1-4), and Unc-89 (H1-4), as well as Mito-GFP (J1-4). Reporters were crossed to wildtype control w^{1118} (A, C, E, G and I 1-4) to establish baseline expression, and then Mettl3 RNAi 5593R to determine the change in expression after loss of Mettl3. Scalebar = 5 µm. DAPI stained nuclei, cyan; phalloidin labelled actin, magenta; GFP-tagged proteins, yellow. 5 thoraxes were imaged each.

(K-P) Quantification of signal intensities of the data shown in A-1 to J-4. Significance determined by t-test, n.s. = not significant; *, p-value < 0.1; **, p-value < 0.01; ***, p-value < 0.001; ****, p-value < 0.0001.



3.1.11 Proteomic analysis of Mettl3 mutant IFMs

We extend our analysis of proteins misregulated after loss of Mettl3 to the entire proteome, we performed a label free mass spectrometry analysis of control w^{1118} and mutant $Mettl3^{\Delta 22-3}$ / Df(3R) Exel6197 IFMs. To validate the data, we first plotted the distribution of pre-imputation intensities for each replicate and sample. All 8 curves had peak intensities around ~27, and were roughly the same height with similar smooth distributions (Fig. 8 A). This shows our data are consistent, and the samples are comparable and thus meaningful.

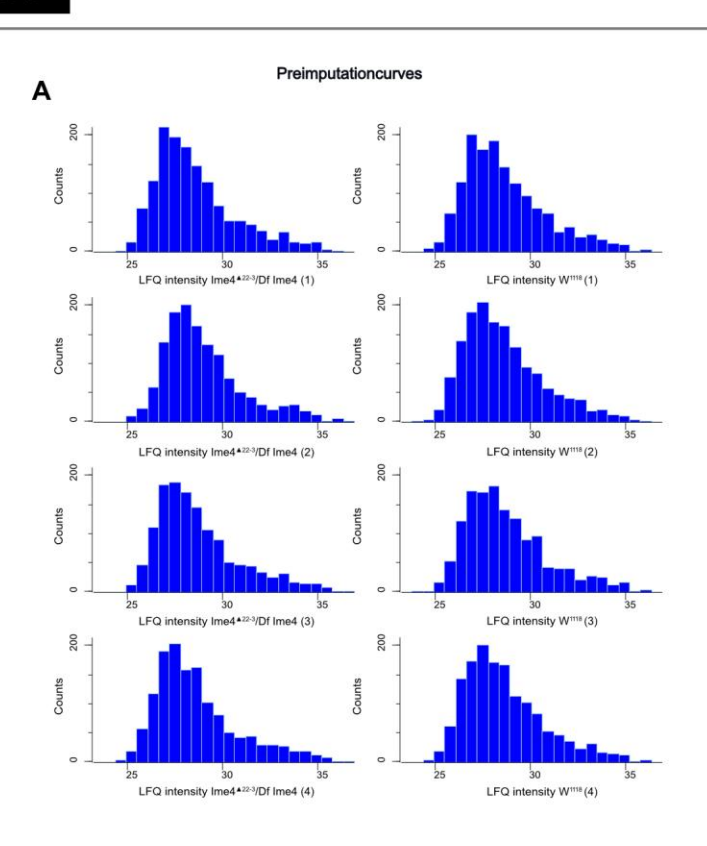
A principal component analysis (PCA) was also done to visualize the variation between the samples and individual replicates of our data in multi-dimensional space (Fig.8 B). A PCA analysis is a dimensionality-reduction approach that standardizes the range of continuous variables, computes a covariance matrix to identify correlations between those variables, generates eigenvectors and eigenvalues to identify the principal components, creates feature vectors of the top principal components that capture the greatest variance, and then recasts the data along the principal component axes. The PCA analysis revealed that 56% of the variance in the proteomics data was captured by the first two principal components, and the wildtype control replicates did cluster tightly and were clearly separated from the mutant replicates in the first dimension. This piece of data thus indicated that the control and the mutant samples were clearly distinct from each other, and can be reliably used for differential protein expression analysis.

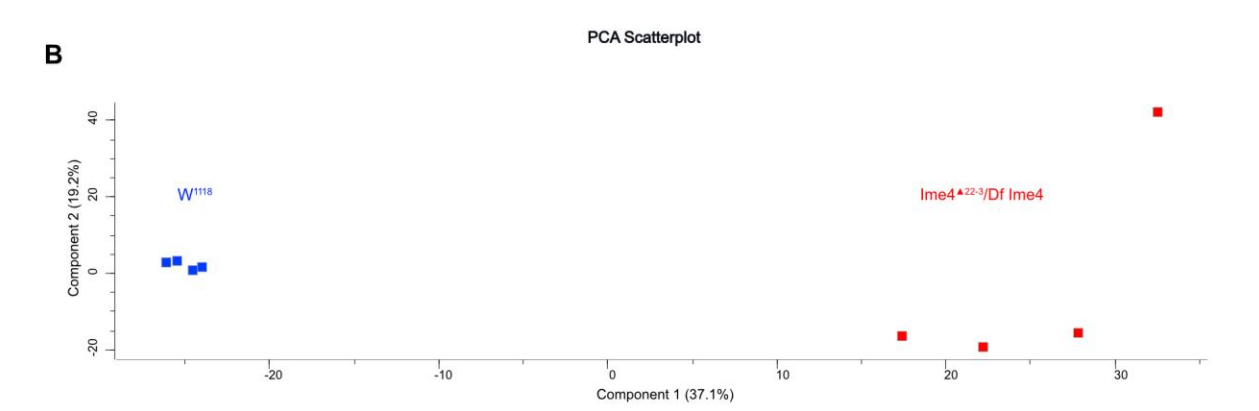
We then performed a differential protein expression analysis based on the LFQ intensity values. We visualized our data with a volcano plot, were we plotted the Difference between the mutant genotype versus the wildtype control on the x-axis, and the significance (-log p-value) on the y-axis (Fig.8 C). The data were distributed in a funnel shape, allowing us to clearly see that several hundred proteins are significantly up- or downregulated in the mutant genotype. Mettl3 was downregulated in the mutant, as expected. We also confirmed multiple sarcomere proteins as downregulated in the proteomics data, and found that genes previously identified as having a muscle-specific RNAi phenotype were significantly downregulated in our data. (Appendix Table)

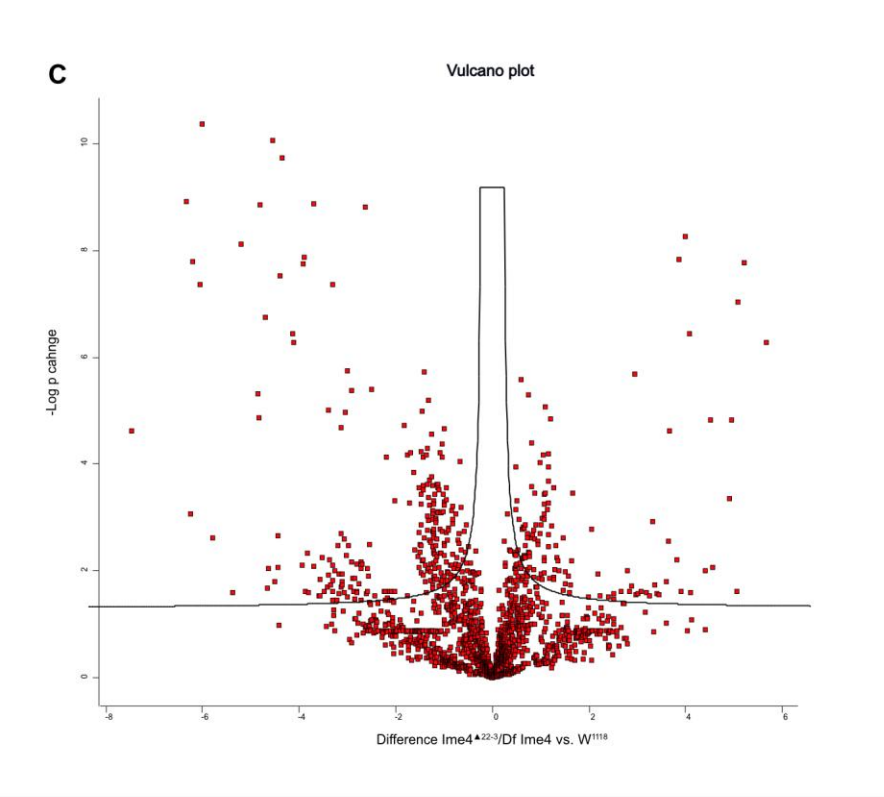
At the time this thesis was written, the data from this experiment still needed to be fully analysed and interpreted. However, we could already draw some conclusions here. We can clearly see significant changes in protein expression in IFMs from Mettl3 mutant animals. This suggests Mettl3 has a function in muscle, and that there are distinct changes in expression of Mettl3 target genes that may underly the observed flightless phenotype. This nicely supports our previous findings regarding altered protein levels in the mutant fly.

Figure 8. Mettl3 mutant flies show significant changes in protein expression.

- (A) Intensity distribution plots for quality control of proteomics samples including the four w^{1118} and four $Mettl3^{\Delta 22-3}/Df$ mutant samples tested in this experiment. The preimputation values show a uniform distribution with their peaks at around ~27 and are roughly the same height and width. For both genotypes in this figure, 50 IFMs went into one replicate. There were 4 replicates, which makes 200 IFMs in total for every genotype.
- **(B)** Principal component analysis shows that the largest component of variance is between control and the mutant samples, which are clearly distinct from each other. The individual biological replicates for each genotype cluster together.
- **(C)** Volcano plot showing that many proteins are differentially expressed between control and Mettl3 mutant ($Mettl3^{\Delta 22-3}/Df$) samples. Difference between the control and mutant samples is plotted on x-axis. The significance is plotted on the y-axis as -log p-value. Smooth lines represent an FDR < 0.05. Zero values (peptides missing in one genotype) were replaced with an intensity value two points lower than the lowest recorded intensity, and thus form the "wings" on the plot. Loss of Mettl3 results in large changes in protein expression in dissected IFM samples.







3.2 Neuronal structure

Previous studies [57-59] as well as our behavioural data from mutant and Elav-Gal4 knockdown experiments suggest that Mettl3 and the m6A pathway play an important role in neuronal development. To determine if there are also neuronal defects in the motor neurons that innervate the IFMs, we analysed the motor neuron axons that innervate IFM from wildtype control, mutant, muscle- and neuronal specific knockdown, muscle- and neuronal specific rescue and all the control lines. Thoraxes were stained for HRP to make the axons, deriving from the motoneurons, visible [30].

Normally, the motor neuron axons fasciculate after exiting the ventral nerve cord and extend centrally in the thorax to the IFMs [60]. After reaching the IFMs, the primary branch forms secondary and higher order branches. Under physiological conditions, those axon branches do not cross or overlap and the overall silhouette looks like a tree. This pattern we also could observe in our wildtype control (Fig. 9 A-1). Strikingly, when we examined the mutant *Mettl3*^{Δ22-3} / *Df(3R)* Exel6197 flies, we saw a dramatic overbranching phenotype. The axons crossed each other frequently and the sparse, tree like silhouette was lost (Fig. 9 B-1). The axon branches were not only more numerous, but also made sharper bends. We conclude that loss of Mettl3 results in an axon overbranching phenotype in the adult IFM motor neurons, consistent with the phenotype reported for larval body wall motor neurons [50].

We next tested if this axon overbranching phenotype is tissue-specific using RNAi. Using Elav-Gal4 knockdown, we saw a comparable pattern with neuronal specific knockdown of Mettl3 (Fig. 9 D-3) to that observed in the mutant (Fig. 9 B-3). The axonal branches grew in a more chaotic manner than in the control and developed more branches. The Mef2-Gal4 muscle knockdown did not display an axon phenotype, and was comparable to the control (Fig. 9 C-3). These data confirm that axon overbranching results from loss of Mettl3 selectively in the neurons.

If Mettl3 function in neurons leads to overbranching, we hypothesized that neuron but not muscle-specific rescue would revert the overbranching phenotype. We therefore checked the motor neuron innervation in the two tissue-specific rescue experiments (Fig. 9 E-1 to F-3).

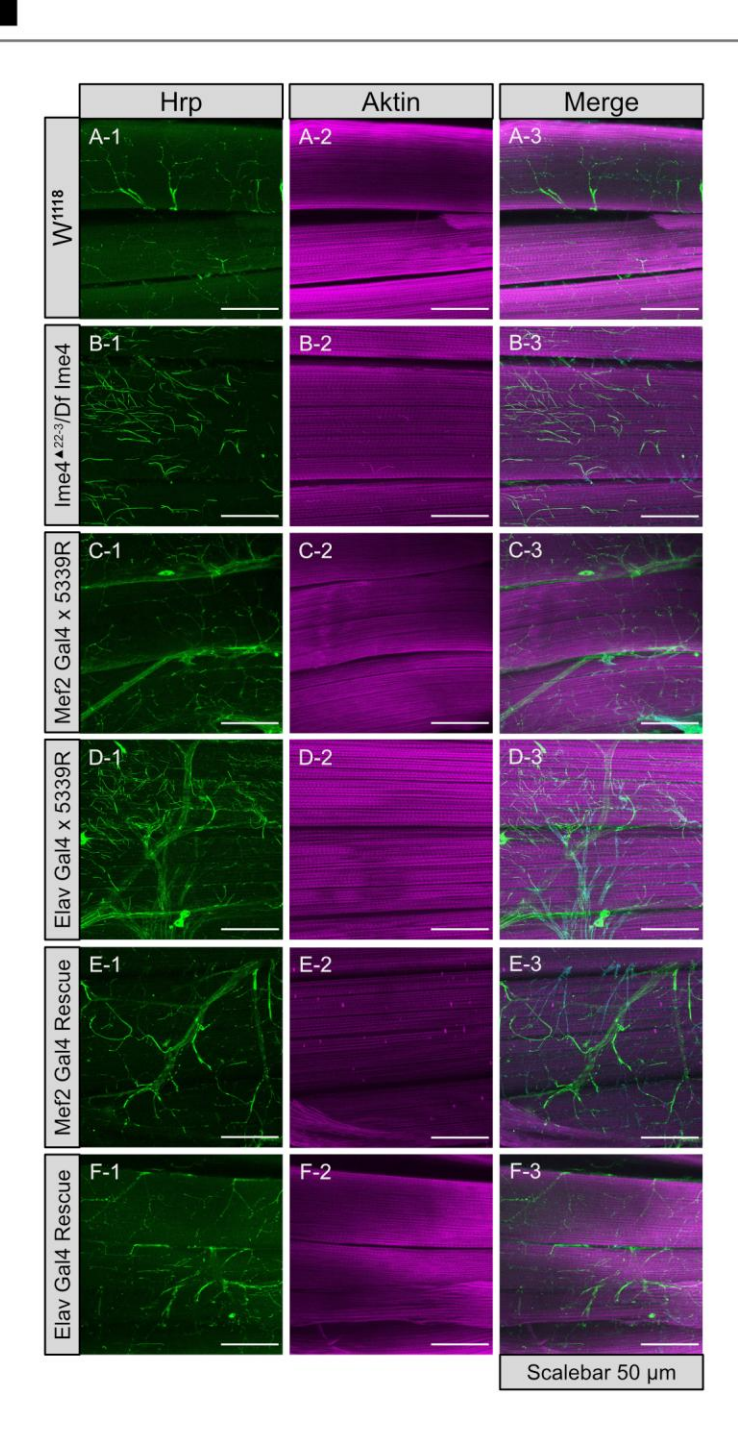
The neuronal specific rescue was indeed more effective and resulted in a near-wildtype branching pattern. Despite the high level of natural variation in motor neuron axon innervation patterns, our data indicate that overbranching contributes to the disrupted IFM function upon loss of Mettl3.

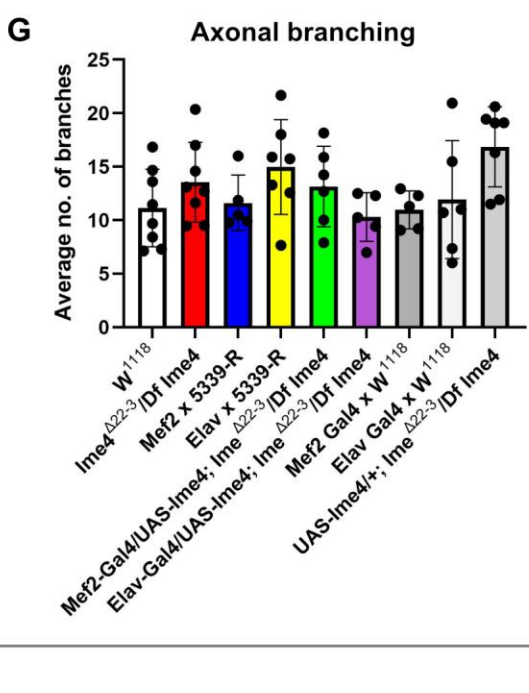
To further analyse the data, we could obtain from those images and calculate the average number of branches one filament has, we performed axonal tracing with the help of Imaris. This task was more difficult than expected, as Imaris had trouble accurately reconstructing the axon structures, especially the primary branches where the axons were thick. Imaris often treated those regions as many single fibres although it was one single, thick fibre. This was most pronounced in physiological control conditions, leading to inflated total axonal length and branch point counts. In addition, backfilling of trachea with DAPI-containing mounting medium could not be distinguished by Imaris from actual axonal staining. Future analysis will be required to generate a more accurate quantitative analysis.

Using the dataset I generate in Imaris, the data were then further analysed and the mean number of branches was quantified and compared between the genotypes (Fig. 9 G). The variance in this data was quite big, and an ANOVA did not reveal a significant difference between samples, as the p-value was 0.0548. We could observe tendencies which supported our visual observations. The mean number of branches was increased in both mutant and the neuronal specific knockdown compared to wildtype. The muscle specific rescue and just the UAS-cassette containing Mettl3 over the mutant background showed elevated results. Matching to our previous findings and assumptions, we saw lower levels in the muscle specific knockdown, the neuronal specific rescue and the drivers crossed to wildtype. In summary, when our data are taken together, we conclude that the loss or depletion of Mettl3 leads to an overgrowth phenotype of motoneuron axons that innervate the IFM of *Drosophila*.

Figure 9. Mettl3 mutants and RNAi knockdown flies exhibit motor neuron axon overbranching.

- (A-F) Maximum projection confocal images of wildtype control w^{1118} (A1-4), $Mettl3^{\Delta22-3}/Df$ mutant (B1-4), muscle specific Mettl3 knockdown (C1-4), neuronal specific knockdown (D1-4), muscle specific rescue (E1-4) and neuronal specific rescue (F1-4) IFM. Mutant IFMs show overbranched axons. Scalebar = 50 μ m. HRP stained axons, cyan; phalloidin labelled actin, magenta. 5 thoraxes were imaged for each genotype.
- **(G)** Quantification of axonal branching of the data shown in A-1 to F-4. Due to technical issues with the tracing software used, this data may not be consistent.





3.3 mRNA-Seq analysis

In this part of the project, we wanted to understand how loss of Mettl3 affects the muscle on the molecular level. To do this, we sequenced and analysed RNA in wildtype and mutant flies to better understand what is happening on the transcriptome level.

3.3.1 mRNA sequencing revealed altered transcriptional patterns of muscle related genes in *Mettl3* mutant flies

To further explore the differences between wildtype and mutant flies, we dissected IFM from both control w^{1118} and mutant $Mettl3^{\Delta 22-3}$ / Df(3R) Exel6197 and performed mRNA-Seq. We then performed a differential expression analysis on the gene level using DESeq2 and on the exon level using DEXSeq. We generated Volcano plots and saw hundreds of genes and exons that were significantly up or down regulated in mutant IFMs (Fig. 10), suggesting that loss of Mettl3 affects a broad set of targets.

To better understand what types of genes were misregulated, we looked for overall trends in the expression of muscle-associated, neuronal, synaptic, and mitochondrial genes. The sets of genes included in the analysis include genes with an RNAi phenotype in muscle (Spletter, eLife, 2018), sarcomere genes (Spletter, eLife, 2018), mitochondrial associated proteins (Yim, NAR, 2020), and genes annotated in Flybase with the GO term "synapse" or "neuromuscular junction". We saw a trend that genes that were reported to have a muscle-specific RNAi phenotype [47], and thus are important for muscle development or function, were downregulated in *Mettl3* mutant IFM (Fig. 10 A). Mettl3 itself was significantly downregulated in the mutant samples, as expected.

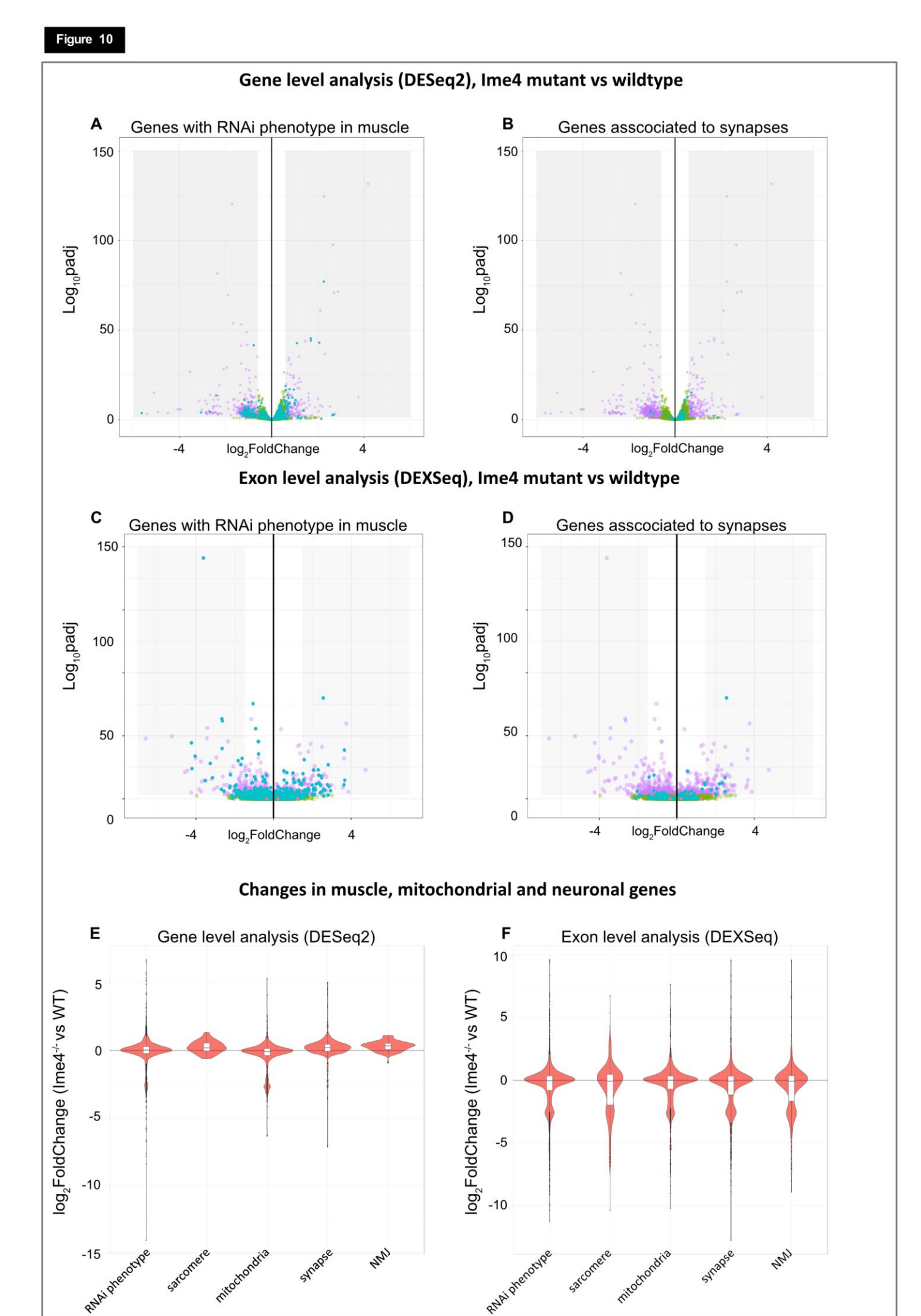
By contrast, strikingly fewer synapse or neuronal associated genes were significantly altered, and those that did change tended to be upregulated (Fig. 10 B). This was also reflected in violin plots, where synapse and neuromuscular junction (NMJ) genes were as a group significantly upregulated (Fig. 10 E). This data supports our earlier conclusions. There are distinct gene expression changes in muscle-related genes, demonstrating a function for Mettl3 in muscle.

Increased expression of NMJ components is consistent with an axon overbranching phenotype.

We performed a similar analysis to understand which genes have exons that are differentially expressed in *Mettl3* mutant muscle. Exons detected by DEXSeq can reflect either alternative splicing, alternative 5' exon use, or alternative 3' exon use. We found that exons from genes with a muscle-specific RNAi phenotype were both up and down regulated (Fig. 10 C), with certain exons of sarcomere genes notably used less frequently than in control IFM (Fig. 10 F). Exons of most synapse genes were not significantly altered, and notably the majority of significantly changed synapse exons were upregulated (Fig. 10 D). Taken together, this data highlights that the loss of Mettl3 causes many changes in exon use and alternative splicing on the transcript level. Those changes affect both muscle and neuronal associated genes, and further support the hypothesis that the m6A-pathway is involved in regulating splicing in IFM.

Figure 10. Mettl3 mutants exhibit altered patterns in gene expression and exon use.

- (A-B) Volcano plots from mRNA-Seq data showing changes in gene expression between control and mutant $Mettl3^{\Delta 22-3}/Df$ IFM. Data was analysed at the level of gene expression with DESeq2. Genes that are significantly misregulated were filtered by a $log_2(fold change) > 0.5$ and a $log_{10}(adjusted p-value) > 0.05$ (purple dots, grey boxes). Data are overlayed with genes associated with an RNAi phenotype in muscle (A, cyan dots) or genes annotated with the GO term "synapse" (B, cyan dots). Genes with an RNAi phenotype in muscle (from Schönbauer $et\ al.$, Nature, 2010) are significantly downregulated in Mettl3 knockdown, while a subset of synaptic genes show increased expression. For those experiments IFMs of 100 flies per genotype were assayed in two replicates.
- **(C-D)** Volcano plots from mRNA-Seq data analysed for changes in exon use using DEXSeq. Significant exons were filtered by a $\log_2(\text{fold change}) > 1.5$ and a $\log_{10}(\text{adjusted p-value}) > 0.05$ (purple dots, grey boxes). Plots were overlayed with genes associated with RNAi phenotype in muscle (C, cyan dots) or genes annotated with the GO term "synapse" (D, cyan dots) in Mettl3 mutant $Mettl3^{\Delta 22-3}$ /Df versus wildtype control IFM. The Mettl3 gene or exons are coloured in red. The fold change between Mettl3 mutant: wildtype control and is plotted on the x-axis as $\log_2(\text{Fold Change})$. The adjusted P-value is plotted on the y-axis ($\log_{10}(1)$).
- **(E-F)** Violin plots showing the changes between wildtype control and Mettl3 mutant on a gene (E) and exon (F) level. On the x-axis the gene sets examine (including genes with an RNAi phenotype in muscle, sarcomere genes, mitochondrial genes, and genes included in GO terms "synapse" and "neuromuscular junction") are labelled. The log₂ fold change in expression is plotted on the y-axis. Each plot is overlayed with the associated box plot in white.



3.3.2 Decreased expression of Mettl3 causes changes in mRNA levels of muscle related proteins

To further extend our understanding of transcriptional changes caused by the loss of Mettl3 and to validate our mRNA-Seq results, we performed qPCR experiments to quantify and compare the amounts of mRNA coding for selected proteins. We dissected IFM from control w^{1118} , mutant $Mettl3^{\Delta 22-3}$ / Df(3R) Exel6197 and muscle-specific RNAi animals (Mettl3- $IR^{N/G-5339}$). Our samples are therefore highly enriched for IFM tissue, although any mRNA transcripts present in the motor neuron axons will also be detected. In both the mutant and the muscle specific knockdown, we saw a decrease of Mettl3 mRNA of greater than 50% (Fig. 11 A). This validates our mutant as well as the knockdown efficiency of our RNAi line.

We then analysed a number of sarcomere proteins, to determine how Mettl3 affects the expression of key structural components of muscle.

The bent (bt) locus encodes Projectin, a large Titin-like protein which is associated with the intermediate filament complex in IFMs and contributes to the stiffness of the muscle. [61]. In agreement with our mRNA-Seq data, we observed a 7-fold increase in bt transcripts in mutant and a 10-fold increase in the muscle specific knockdown (Fig. 11 B). Act88F is the Actin isoform expressed specifically in IFM which is the major component of the thin filament [62]. Act88F (Fig. 7 A1-B4), qPCR showed a significant decrease of ~90% in *Act88F* expression in both the mutant and the muscle specific knockdown (Figure 9 D). These findings were supported by the results obtained from the Fosmid reporter experiments; here we also saw a significant decrease in intensity in mutant IFM. (Fig. 7 B-3 and K) Flightin (FIn) is a thick-filament associated protein expressed specifically in differentiated IFM that is necessary for flight and sarcomere structure [63]. Consistent with the findings from the Fln Fosmid reporter (Fig. 7), fln mRNA levels were around 80% reduced in mutant and about 60% less in the RNAi knockdown (Fig. 11 C). These results are consistent with both our mRNA-Seq and our Fosmid-reporter data, and show that a decrease or loss of Mettl3 expression alters the expression of key muscle-related mRNAs and proteins.

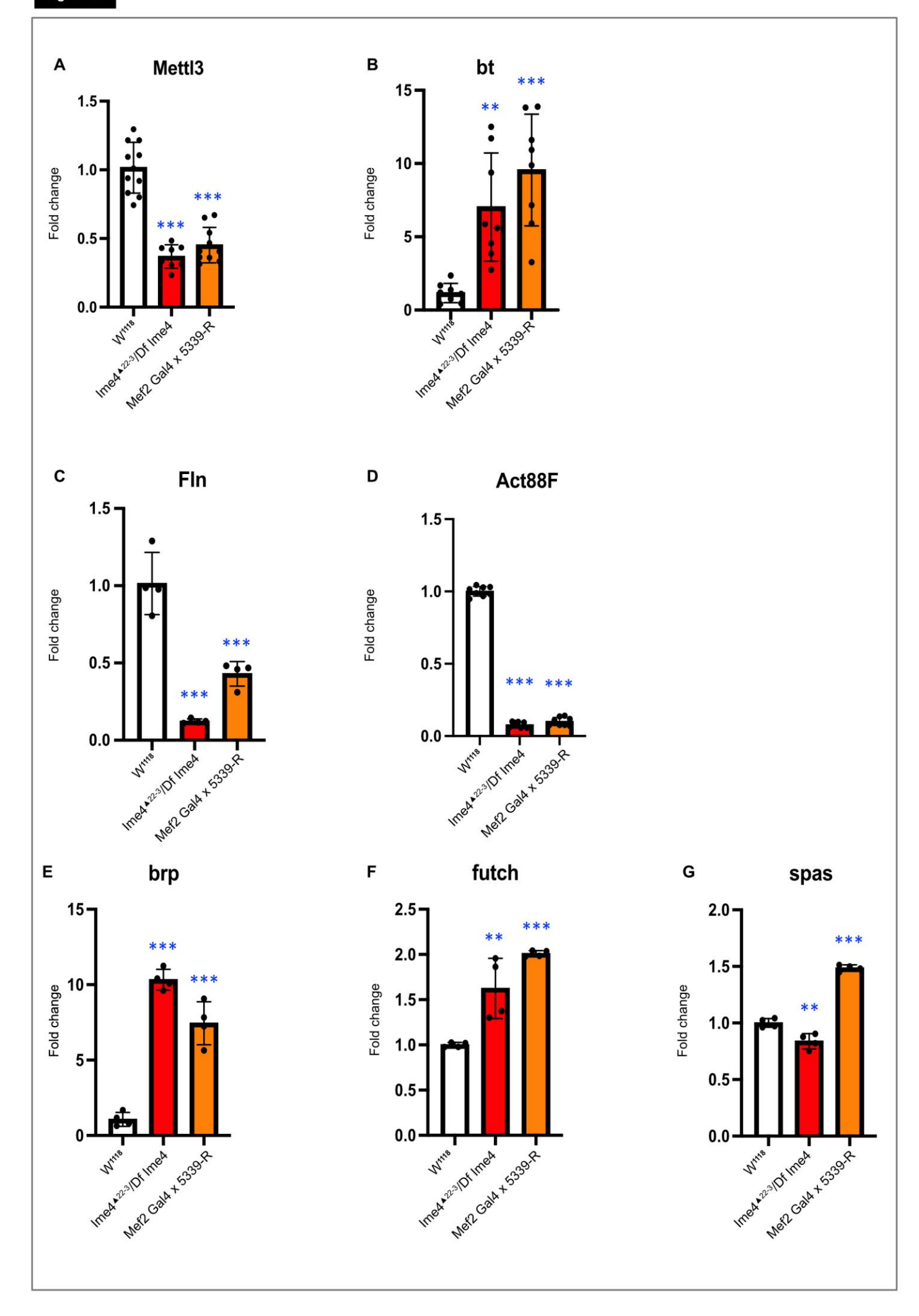
3.3.3 Decreased expression of Mettl3 in an increase in the mRNAs of neuronal- and synaptic related proteins

Our results above demonstrated that IFM motor neuron axons are over branched (Fig. 9) and our mRNA-Seq data showed that mRNA levels of synaptic components are increased after loss of Mettl3 (Fig. 10). To validate this finding, we performed RT-qPCR for several neuronal or synaptic targets. Bruchpilot (Brp) is a cytoskeletal protein which contributes to size regulation of synaptic vesicles, calcium channel clustering, and is critical for the structural integrity of the T-bar region within synapses. [64] In Mettl3 mutant flies, where mRNA levels of Mettl3 were strongly decreased, we measured an approximately 10-fold increase of mRNA coding for *brp*, while in the muscle-specific RNAi knockdown we observed about a 7-fold increase (Fig. 11 E). Futch is a microtubule binding protein involved in the formation of synaptic buttons at the neuromuscular junction [65]. *futch* expression saw a 1.6-fold increase in mutant and a 2-fold increase in the RNAi knockdown (Fig. 11 F).

Spastin (Spas) is a protein which assembles into hexamers and severs microtubules along their lengths, contributing to neuronal axon transport, synapse formation and dendrite arborization [66]. Although *Spas* expression was not significantly affected in the mutant IFM, we detected a 1.5-fold increase in the muscle specific RNAi knockdown (Fig. 11 G). Our experiments therefore confirm our mRNA-Seq results and show that depletion of Mettl3 results in increased expression of synaptic components including *brp*, *Spas*, and *futch*. These results are consistent with the over branching phenotype we describe in Mettl3 mutants.

Figure 11. Mettl3 Mutants and RNAi knockdown flies show significant changes in the amount of mRNA for selected proteins.

(A-G) Semi-quantitative RT-qPCR analysis of gene expression. Plots quantifying the fold change in mRNA expression. Control w^{1118} was normalized to 1. Significance determined by ANOVA and posthoc Tukey, n.s. = not significant; **, p-value < 0.01; ***, p-value < 0.001. For those experiments 200 IFMs of each genotype were assayed in two biological replicates of 100 IFMs each. Three to five technical replicates were performed from each biological replicate.



3.3.4 Decreased expression of Mettl3 causes defects in alternative splicing and isoform expression of Titin-like protein Projectin

To validate the defects in exon usage we detected in our mRNA-Seq data, we performed semi-quantitative RT-PCR experiments. Here we were especially interested in possible isoform switches. Although this part of the study was not yet completed when this thesis was written, there was already one particular result complete enough to be presented in this work. Projectin, encoded by the *bent* (*bt*) gene, is a large, Titin-like protein which is associated with the intermediate filaments and contributes to the stiffness of IFM [61]. In *Drosophila* there are five annotated splice isoforms of this protein, including a short version with a short PEVK domain found exclusively in IFM and long versions that include additional PEVK domain exons which are associated with tubular muscles [67]. It has been shown that expression of long Projectin isoforms in IFM results in reduced stretch activation and altered IFM kinetics [68]. Newer publications show, that a knock downs for bent are lethal [47]

We designed forward and reverse primers that span the alternatively-spliced PEVK region of *bt*, from exon 14 to exon 25 of that gene. The short isoform of *bt* contains exons 14-16-25 and has an RT-PCR product with a length of around 181 base pairs. The long isoforms of *bt* expressed in adult flies, on the other hand, contain additional exons including 14-15-16-17-18-20-21-25 and produce a RT-PCR products that are 800 and 900 base pairs long (Fig.12 A). In IFM from control flies, we could only detect the band for the short isoform at around 100 base pairs (Fig. 12 B).

This band was also visible in the Mettl3 mutant and the knockdown samples, but in addition we saw a band at 800 base pairs and a prominent band at 900 base pairs (Fig. 12 B). Quantification of the data revealed a significant decrease in the use of the short isoform in both mutant and knockdown IFM, and a corresponding increase in the use of the longer, tubular isoforms (Fig.12 C). These results show that decreased expression or loss of Mettl3 results in the expression of tubular muscle specific isoforms of *bt* in IFM, which is not physiological.

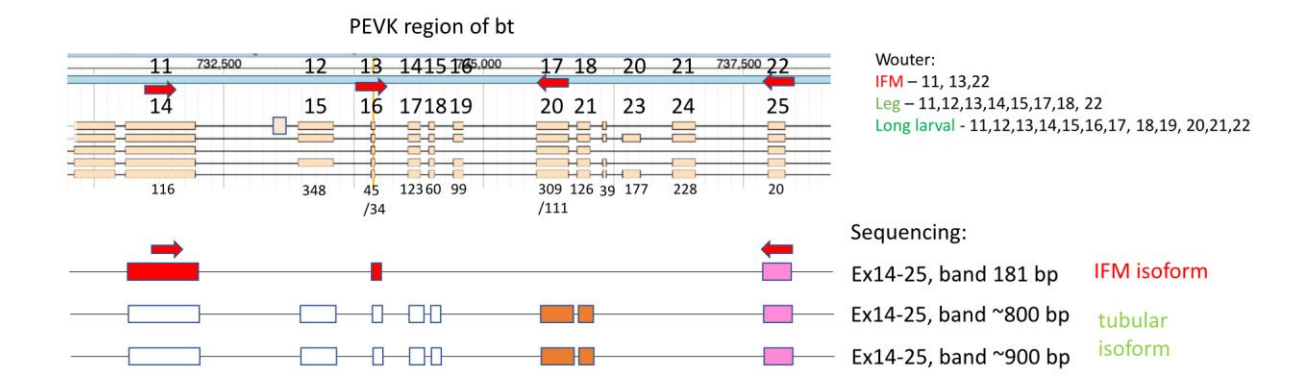
This shows that Mettl3 and hence the m6A-pathway is involved in the correct splicing of *bt* in IFM, and further identifies a mechanism that underlies the flight defect observed in Mettl3 mutant and RNAi knockdown flies.

Figure 12. Mettl3 controls an isoform switch in Titin-like Projectin.

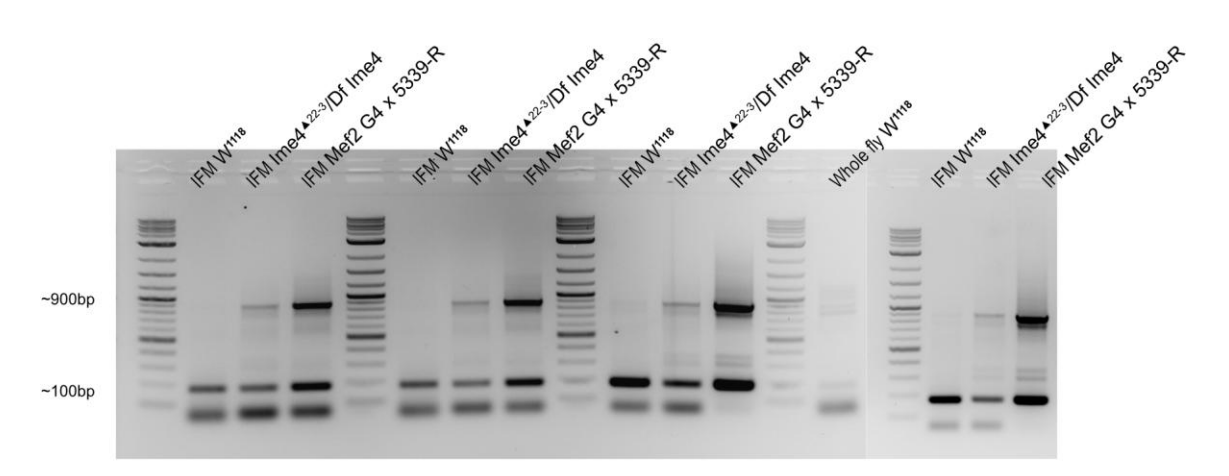
(A) Plot showing the exons in the PEVK region of Projectin (*bent*, *bt*). Red arrows stand for the primers used in this experiment. The short IFM isoform of *bt* contains exons 14, 16 and 25. The long, tubular isoforms contain exons 14-15-16-17-18-20-21-25.

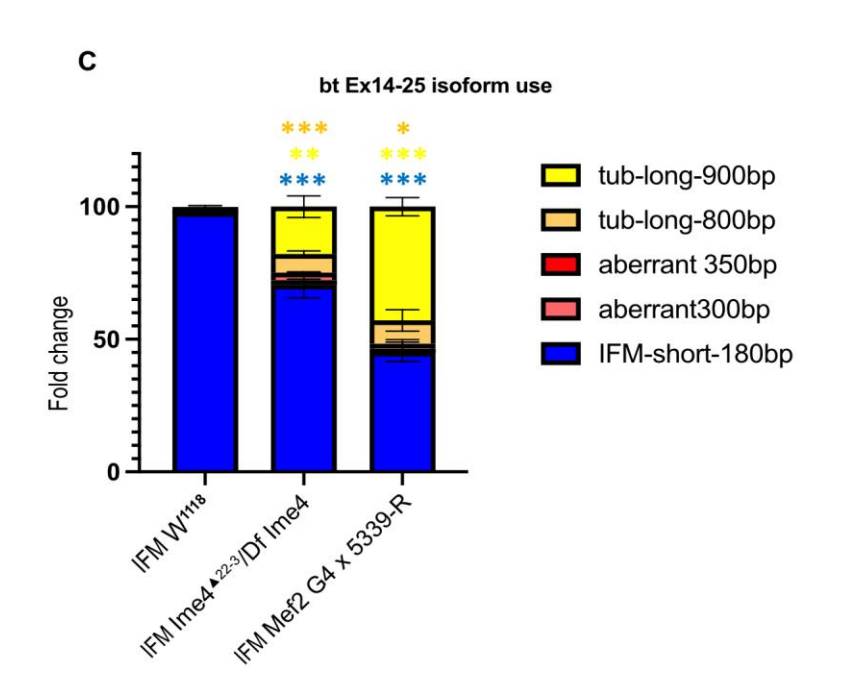
- **(B)** Gel image of the PCR result with primers for exon 14-25 for dissected IFMs from wildtype control, Mettl3 mutant and Mettl3 knockdown. Wildtype control only shows one band at around 100 basepairs, whereas the mutant and the knockdown probes show an additional band at around 900 basepairs. For those experiments 200 IFMs from flies of each genotype were assayed in one replicate.
- **(C)** Plot quantifying the isoform use from the data obtained in B. Significance determined by ANOVA with posthoc Tukey, n.s. = not significant; *, p-value < 0.1; **, p-value < 0.01; ***, p-value < 0.001; ****, p-value < 0.0001.





B RT-PCR gel for exon 14-25 primers





4. Discussion

In this study, we identified a novel function for the m6A pathway in *Drosophila* indirect flight muscle. We show by tissue-specific RNAi and tissue-specific rescue that Mettl3 has an intrinsic function in muscle, as well as a function in the IFM motor neurons. Our proteomics and mRNA-Seq data reveal changes in expression of many muscle related genes. We confirm changes in expression of Act88F, Fln, Unc-89 (Obscurin), and Projectin (*bent*) using GFP-tagged Fosmid reporters or RT-qPCR. We moreover confirm an isoform switch from short to long Projectin isoforms that causes flightlessness. The data presented here thus extend our understanding of the role of the m6A pathway and Mettl3 in muscle and demonstrate the conservation of Mettl3 pathway from flies to mammals.

4.1 Flightlessness of Mettl3 mutants is not a purely neuronal phenotype

Previous studies have suggested that the flightless phenotype, impaired climbing ability and held-out wings observed in Mettl3 mutants are of a neuronal nature [26, 57]. In this study we found that the loss of Mettl3 in mutant flies indeed leads to over branching and axon overgrowth of IFM motor neurons (Fig. 9). We further show increased mRNA levels coding for the proteins Bruchpilot, Futch and Spas, which are key synaptic components [64-66] (Fig. 11). These data are consistent with previous studies in *Drosophila* larvae that showed over branching and increased bouton formation in Mettl3-mutant sensory neurons [50, 69]. Further, mis-splicing of *trio* leading to an imbalance in Rac and RhoGTPase activity has been implicated in axon branching defects in class IV sensory neurons in Nab2 mutants with aberrant m6A methylation [70]. Future experiments will be necessary to determine if Mettl3 activity helps promote axon pruning or alternatively limits axon branch formation in both the larval and adult peripheral nervous system. This data indicates that the m6A pathway is involved in the normal development of the adult nervous system in *Drosophila*.

Our data demonstrate that Mettl3 activity in both the muscle and neurons contribute to observed behavioural defects in Mettl3 mutants. Using tissue specific RNAi, we showed that flies performed motor tasks like climbing worse when

Ime4 was knocked down specifically in neurons, but climbing was not as strongly affected when Mettl3 was knocked down in muscle (Fig. 4 B). The same tendency was also observed for the held-out wings phenotype (Fig. 4 C). By contrast, loss of flight ability was more pronounced with muscle-specific knockdown of Mettl3 than with neuronal-specific knockdown (Fig. 4 A). One possible explanation is that fibrillar IFM, unlike other muscle-fibre types like tubular muscles, are stretchactivated, asynchronous, and can oscillate at high frequencies autonomously once activated [71]. While fibrillar IFM may require neuronal activity to initiate flight, it is able to contract independent without sustained neuronal input. Tubular muscles, like leg or jump muscle, are synchronous and their contraction is dependent on continuous and sustained neuronal input. This type of relationship between muscles and motor neuron function may be reflected in different human disorders, for example facioscapulohumeral dystrophy (FSHD), oculopharyngeal muscular dystrophy, or limb-girdle muscular dystrophy, where molecular characteristics of different sets of muscles make them more susceptible and show differential levels of involvement in the disease [72-74]. Taken together our data show that behavioural defects such as flight involve Mettl3 function in both neurons and muscle.

4.2 Mettl3 is required in muscle to regulate sarcomere dimensions in IFM

Recent studies in mammals have identified a function for Mettl3 in regulation muscle hypertrophy [75], in cardiac development [76], and in myoblast division and differentiation [77]. Our data demonstrate that Mettl3 also plays an important role in *Drosophila* indirect flight muscle, illustrating a conserved function for the m6A pathway in muscle development. Our confocal data revealed altered sarcomere structure in Mettl3 mutant IFM, where the sarcomeres were significantly longer in the mutant than in the wildtype control (Fig. 1, I1-J4). Sarcomere dimensions were also altered in the muscle specific knockdown and appeared either too be too long or too short (Fig. 4 D1-G4).

These data suggest that misregulation of Mettl3 affects sarcomere length, and may lead to an imbalance in isoform-specific splicing leading to hypercontraction of the muscle fibres. The appearance of zebra-bodies within the sarcomeres indicates abnormal thin-filament assembly or stability. Notably those changes in the sarcomere dimensions could not be found in the neuronal specific

knockdown, and thus must derive from loss or depletion of Mettl3 within the muscle itself.

Also, the circumstance, that this cellular defect can be rescued tissue specifically as we have shown again highlights the muscular nature of this cellular phenotype.

Taken together also this part of our experiments showed once again, that the m6A-pathway is involved in the natural development of working muscle fibres.

Recent studies described, that in mice, Mettl3 is involved in the myostatin pathway on a posttranscriptional level. This pathway is critical for the control of muscle size and growth [75]. Also in mice, Mettl3 is furthermore involved in proliferation and differentiation of muscle stem cells. Hence it controls myogenesis and regeneration of mammalian muscle tissue [78, 79]. In other studies, it is stated, that Mettl3 supresses muscle specific miRNAs in C2C12 myoblasts and plays an important role in their differentiation [31].

4.3 Mettl3 and the m6A pathway regulate alternative splicing in IFM

When we performed antibody staining for Mettl3, we could see a clear nuclear signal in IFM, suggesting Mettl3 may play a role in the nucleus. Our RNA sequencing from dissected IFMs revealed many genes coding for muscle related proteins that are changed in the Mettl3 mutants. Some of these are changed at the level of gene expression, while others displayed differential exon use in muscle related genes. This data indicates that Mettl3 may play a role in the nucleus in muscle tissue to regulate alternative splicing. Mettl3 has also been reported to regulate splicing during germline development, notably controlling sex differentiation through regulation of sex-specific splicing of Sxl [26]. Mettl3 in mammals is also reported to regulate alternative splicing. For instance, it has been published, that Mettl3 and its m6A mark are involved in alternative splicing events in pig skeletal muscles. Here they could contribute to the differentiation between oxidative and glycolytic muscles [80]. Apart from alternative splicing in muscle tissue it has also been suggested, that Mettl3 also regulates breast cancer-associated alternative splicing switches [81]. Furthermore, Mettl3 seems also to be involved in mammalian fertility due to alternative splicing. It has been found out, that Mettl3 regulates spermatogonial differentiation and meiosis in mice [82].

Our RT-PCR experiments moreover showed an isoform switch of *bent*, which encodes the Titin-like protein Projectin and is required for physiological function of IFM in *Drosophila* [61]. There are multiple splice isoforms of *bent*, but the distinction between long and short isoforms is of physiological relevance. Tubular muscles express long isoforms of Projectin, while IFMs express short isoforms which are thought to contribute to the high passive stiffness of IFM tissue. Short Projectin isoform expression is also essential for stretch-activation and cannot be compensated by longer isoforms [67, 68]. It is likely that this isoform switch alone strongly contributes to the flightless phenotype in mutant as well as in muscle specific knockdown flies. Muscles are a highly complex and organized tissue; thus, they are sensitive to wrong isoforms.

4.4 mRNA transcript-level changes in Mettl3 mutant IFM are reflected in the proteome

Our data showed corresponding changes on the mRNA and proteomic level, likely capturing changes both on transcriptional level as well as any effect on mRNA stability or translation. Proteomics analysis revealed that many peptides and hence proteins are changed in the mutant background. Immunofluorescence microscopy of GFP-tagged Fosmid reporter lines confirmed a significant decrease in expression of muscle associated proteins like Myofilin and Fln, which were also downregulated in mRNA-Seg and proteomics data from muscle specific Mettl3 knockdown IFM. Furthermore, we could show shifts in expression of specific categories of proteins, such as mitochondrial or sarcomere related proteins. For example, expression of sarcomere related proteins as well as synaptic proteins increased more strongly on the proteomics level than on the gene level. This effect could be explained by the function of the m6A-pathway in translation [22]. In fact, many m6A target sites have been identified within 5'-UTRs of genes in both vertebrates and *Drosophila* [22, 27]. Methylation in this region could be read by YTH reader proteins associated with translation complexes, NMD machinery, or mRNA trafficking, and either inhibit or promote the eventual translation of a particular protein [83].

All the proteins analysed here by Fosmid reporter lines were in fact previously identified as direct-targets of the m6A-pathway by meRIP [29]. In future experiments that are beyond the scope of this work, it would be interesting to take a

closer look into the translation process itself, for example, to pull down ribosomes in mutant and wildtype flies and analyse which mRNAs get in fact translated. This would increase our insight into potential cytoplasmic roles of the m6A pathway in IFM.

One of the genes misregulated in our data illustrates the potentially complex relationships between alternative splicing, proteomics, and Mettl3 function. The GFP-tagged Fosmid reporter line for Myofilin showed a decrease in expression, but both RT-PCR and proteomics showed quite the opposite, an increase of Myofilin expression. A check of the position of the GFP tag itself showed that it is located just before the 5'-UTR of *Mf* exon 1 and is isoform specific. *Mf* encodes 17 transcripts, only 5 of which are annotated to use this particular termination (Flybase). RT-PCR also showed that in the mutant background, there seems to be yet another isoform switch in Mf expression from the exon1-exon3 event (which would be the GFP-tagged isoform) to the exon1-exon2-exon3 event (which would not include the GFP-tag because exon2 encodes a stop codon upstream of the GFP). When we looked for individual peptides within our proteomics data, we found one which covered the exactly the splice junction area between exon2 and exon3 which was significantly upregulated in Mettl3 RNAi as compared to control IFM in the proteomic analysis. Thus, we saw a decrease with our Fosmid reporter approach but an increase in expression with our other two assay methods. This highlights how apparent inconsistencies between different assays for gene and protein expression can reveal biological regulatory mechanisms impacted the Mettl3 activity and m6A pathway function.

4.5 Conclusion

The results discussed in this thesis lead us to the conclusion that the m6A-path-way is indeed involved in muscle as well as neuronal tissue is *Drosophila*. The flightless phenotype of *Mettl3* mutant flies, based on our data, results from IFM defects including isoform switches of key sarcomere components, altered sarcomere morphology, and possible mitochondrial alterations. The flightless phenotype is further exacerbated by over branching of IFM motor neurons. Our data

therefore highlight a role for Mettl3 and m6A modification in both tissues, and provide an example how tissue-specific phenotypes synergize to produce organism-level behavioural defects.

There are several limitations of our study, and a lot of future experiments are conceivable. While some analysis of the sequencing and massSpec data was completed, the data still needs to be fully analysed and to be examined in the context of our existing work. This may reveal additional signatures or trends in the data that are not discussed in this work. We have tested a number of potential targets by RT-PCR, but a more extensive list of targets could be tested by RT-PCR. The differences in mRNA versus protein level expression for the selected targets could also be assayed by Western Blot, to better define the connection between RNA and protein expression levels. This would also likely shed more light on which targets are regulated at the level of translation or mRNA stability in the cytoplasm, versus those targets whose alternative splicing is regulated in the nucleus. There are also a lot more genes with potential isoform switches to be confirmed and further investigated. Here it would be particularly interesting to analyse also mitochondrial genes. Ongoing work in the Spletter lab will seek to address some of these open questions regarding Mettl3 and m6A pathway function in IFMs.

The data presented here extends our knowledge about the m6A pathway in muscle tissue. Our work identifies important roles for Mettl3 in regulating alternative splicing of structural genes as well as potentially regulating development shifts in expression through regulating the stabilization of select transcripts during myogenesis.

Although our findings were made in a model organism, *Drosophila* is an excellent model organism to understand disease also in humans due to genetic conservation [43]. Existing reports of Mettl3 function during hypertrophy and cardiomyogenesis also indicate an important function for Mettl3 during growth and remodelling of human muscle [84]. Further, the m6A pathway has been reported to play an important role in heart diseases and muscle dystrophy in humans [43], indicating that our findings are disease relevant. Our work contributes to a better understanding of Mettl3 function in muscle, and possibly may one day contribute to development of new therapy approaches for diseases affected by abnormal m6A pathway activity.

References

1. Spletter ML, Barz C, Yeroslaviz A, Zhang X, Lemke SB, Bonnard A, Brunner E, Basler GCK, Schnorrer BHHF: A transcriptomics resource reveals a transcriptional transition during ordered sarcomere morphogenesis in flight muscle. *eLife* 2018.

- Speckmann E-J, Hescheler J, Köhling R: Physiologie, 6 edn; 2013.
- 3. Bate M, Rushton E, Currie DA: Cells with persistent twist expression are the embryonic precursors of adult muscles in Drosophila. *Development* 1991, 113(1):79-89.
- 4. Kim JH, Jin P, Duan R, Chen EH: **Mechanisms of myoblast fusion during muscle development**. *Current Opinion in Genetics & Development* 2015, **32**:162-170.
- 5. Weitkunat M, Schnorrer F: **A guide to study Drosophila muscle biology**. *Methods* 2014, **68**(1):2-14.
- 6. Weitkunat M, Kaya-Copur A, Grill SW, Schnorrer F: **Tension and force-resistant attachment are essential for myofibrillogenesis in Drosophila flight muscle**. *Curr Biol* 2014, **24**(7):705-716.
- 7. Lemke SB, Schnorrer F: **Mechanical forces during muscle development**. *Mechanisms of development* 2017, **144**(Pt A):92-101.
- 8. Baylor SM, Hollingworth S: Intracellular calcium movements during excitation-contraction coupling in mammalian slow-twitch and fast-twitch muscle fibers. *J Gen Physiol* 2012, **139**(4):261-272.
- 9. Schiaffino S, Reggiani C: **Fiber types in mammalian skeletal muscles**. *Physiological reviews* 2011, **91**(4):1447-1531.
- 10. Murgia M, Nogara L, Baraldo M, Reggiani C, Mann M, Schiaffino S: **Protein profile of fiber types in human skeletal muscle: a single-fiber proteomics study**. *Skelet Muscle* 2021, **11**(1):24.
- Murgia M, Toniolo L, Nagaraj N, Ciciliot S, Vindigni V, Schiaffino S, Reggiani C, Mann M: Single Muscle Fiber Proteomics Reveals Fiber-Type-Specific Features of Human Muscle Aging. Cell Rep 2017, 19(11):2396-2409.
- 12. Nikonova E, Kao SY, Spletter ML: **Contributions of alternative splicing to muscle type development and function**. *Seminars in cell and developmental biology* 2020, **104**:65-80.
- 13. Lüllmann-Rauch R: **Histologie**, 5 edn; 2015.
- 14. Peckham M, Molloy JE, Sparrow JC, White DC: Physiological properties of the dorsal longitudinal flight muscle and the tergal depressor of the trochanter muscle of Drosophila melanogaster. *J Muscle Res Cell Motil* 1990, **11**(3):203-215.
- 15. Dickinson M: **Insect flight**. *Current Biology* 2006, **16**(9):309-314.
- 16. Josephson RK, Malamud JG, Stokes DR: **Asynchronous muscle: a primer**. *The journal of experimental biology* 2000, **203**(18):2713-2722.
- 17. Spletter ML, Barz C, Yeroslaviz A, Schonbauer C, Ferreira IR, Sarov M, Gerlach D, Stark A, Habermann BH, Schnorrer F: **The RNA-binding protein Arrest (Bruno) regulates alternative splicing to enable myofibril maturation in Drosophila flight muscle**. *EMBO reports* 2015, **16**(2):178-191.
- 18. Schonbauer C, Distler J, Jahrling N, Radolf M, Dodt HU, Frasch M, Schnorrer F: **Spalt** mediates an evolutionarily conserved switch to fibrillar muscle fate in insects. *Nature* 2011, **479**(7373):406-409.
- 19. Spletter ML, Schnorrer F: **Transcriptional regulation and alternative splicing cooperate in muscle fiber-type specification in flies and mammals**. *Experimental cell research* 2014, **321**(1):90-98.

20. Guo W, Bharmal SJ, Esbona K, Greaser ML: **Titin diversity--alternative splicing gone wild**. *Journal of biomedicine and biotechnology* 2010(Special Issue).

- 21. Linke WA, Kulke M, Li H, Fujita-Becker S, Neagoe C, Manstein DJ, Gautel M, Fernandez JM: **PEVK domain of titin: an entropic spring with actin-binding properties**. *Journal of structural biology* 2002, **137**(1-2):194-205.
- 22. Balacco DL, Soller M: **The m(6)A Writer: Rise of a Machine for Growing Tasks**. *Biochemistry* 2019, **58**(5):363-378.
- 23. Modrek B, Lee C: A genomic view of alternative splicing. *Nature genetics* 2002, **30**(1):13-19.
- 24. Anreiter I, Mir Q, Simpson JT, Janga SC, Soller M: **New Twists in Detecting mRNA Modification Dynamics**. *Trends Biotechnology* 2021, **39**(1):72-89.
- 25. Gilbert WV, Bell TA, Schaening C: **Messenger RNA modifications: Form, distribution, and function**. *Science* 2016, **352**(6292):1408-1412.
- 26. Haussmann IU, Bodi Z, Sanchez-Moran E, Mongan NP, Archer N, Fray RG, Soller M: m(6)A potentiates SxI alternative pre-mRNA splicing for robust Drosophila sex determination. *Nature* 2016, **540**(7632):301-304.
- 27. Dominissini D, Moshitch-Moshkovitz S, Schwartz S, Salmon-Divon M, Ungar L, Osenberg S, Cesarkas K, Jacob-Hirsch J, Amariglio N, Kupiec M *et al*: **Topology of the human and mouse m6A RNA methylomes revealed by m6A-seq**. *Nature* 2012, **485**(7397):201-206.
- 28. Wei CM, Moss B: Nucleotide sequences at the N6-methyladenosine sites of HeLa cell messenger ribonucleic acid. *Biochemistry* 1977, **16**(8):1672-1676.
- 29. Wang Y, Zhang L, Ren H, Ma L, Guo J, Mao D, Lu Z, Lu L, Yan D: **Role of Hakai in m(6)A modification pathway in Drosophila**. *Nature Communications* 2021, **12**(1):2159.
- 30. Worpenberg L, Paolantoni C, Longhi S, Mulorz MM, Lence T, Wessels H-H, Dassi E, Aiello G, Sutandy FXR, Scheibe M *et al*: **Ythdf is a N6-methyladenosine reader that modulates Fmr1 target mRNA selection and restricts axonal growth in Drosophila**. *Embo journal* 2021, **40**.
- 31. Diao LT, Xie SJ, Lei H, Qiu XS, Huang MC, Tao S, Hou YR, Hu YX, Sun YJ, Zhang Q et al: METTL3 regulates skeletal muscle specific miRNAs at both transcriptional and post-transcriptional levels. Biochemical and Biophysical Research Communications 2021, 552:52-58.
- 32. Bawankar P, Lence T, Paolantoni C, Haussmann IU, Kazlauskiene M, Jacob D, Heidelberger JB, Richter FM, Nallasivan MP, Morin V *et al*: **Hakai is required for stabilization of core components of the m(6)A mRNA methylation machinery**. *Nature Communications* 2021, **12**(1).
- 33. Knuckles P, Lence T, Haussmann IU, Jacob D, Kreim N, Carl SH, Masiello I, Hares T, Villaseñor R, Hess D *et al*: **Zc3h13/Flacc is required for adenosine methylation by bridging the mRNA-binding factor Rbm15/Spenito to the m(6)A machinery component Wtap/FI(2)d**. *Genes and development* 2018, **32**(5-6):415-429.
- 34. Bujnicki JM, Feder M, Radlinska M, Blumenthal RM: Structure prediction and phylogenetic analysis of a functionally diverse family of proteins homologous to the MT-A70 subunit of the human mRNA:m(6)A methyltransferase. *Journal of Molecular Evolution* 2002, 55(4):431-444.
- 35. Iyer LM, Zhang D, Aravind L: Adenine methylation in eukaryotes: Apprehending the complex evolutionary history and functional potential of an epigenetic modification. *Bioessays* 2016, **38**(1):27-40.
- 36. Jia G, Fu Y, Zhao X, Dai Q, Zheng G, Yang Y, Yi C, Lindahl T, Pan T, Yang YG et al: N6-methyladenosine in nuclear RNA is a major substrate of the obesity-associated FTO. Nature chemical biology 2011, 7(12):885-887.
- 37. Zhang S, Zhao BS, Zhou A, Lin K, Zheng S, Lu Z, Chen Y, Sulman EP, Xie K, Bogler O et al: m(6)A Demethylase ALKBH5 Maintains Tumorigenicity of Glioblastoma Stem-

- like Cells by Sustaining FOXM1 Expression and Cell Proliferation Program. Cancer Cell 2017, **31**(4):591-606.
- 38. Theler D, Dominguez C, Blatter M, Boudet J, Allain FH: **Solution structure of the YTH domain in complex with N6-methyladenosine RNA: a reader of methylated RNA**. *Nucleic acids research* 2014, **42**(22):13911-13919.
- Wang X, Lu Z, Gomez A, Hon GC, Yue Y, Han D, Fu Y, Parisien M, Dai Q, Jia G *et al*: **N6-methyladenosine-dependent regulation of messenger RNA stability**. *Nature* 2014, **505**(7481):117-120.
- 40. Lence T, Soller M, Roignant JY: **A fly view on the roles and mechanisms of the m(6)A mRNA modification and its players**. *RNA Biology* 2017, **14**(9):1232-1240.
- 41. Matthews BJ, Vosshall LB: **How to turn an organism into a model organism in 10 'easy' steps**. *Journal of experimental biology* 2020, **223**(Pt Suppl 1).
- 42. Fernandez-Moreno MA, Farr CL, Kaguni LS, Garesse R: **Drosophila melanogaster as a model system to study mitochondrial biology**. *Methods in molecular biology* 2007, **372**:33-49.
- 43. Taghli-Lamallem O, Plantie E, Jagla K: Drosophila in the Heart of Understanding Cardiac Diseases: Modeling Channelopathies and Cardiomyopathies in the Fruitfly. *Journal of cardiovascular development and disease* 2016, **3**(1):7.
- 44. Jawkar S, Nongthomba U: Indirect flight muscles in Drosophila melanogaster as a tractable model to study muscle development and disease. *The international journal of developmental biology* 2020, **64**(1-2-3):167-173.
- 45. Kozopas KM, Nusse R: Direct flight muscles in Drosophila develop from cells with characteristics of founders and depend on DWnt-2 for their correct patterning. *Developmental biology* 2002, **243**(2):312-325.
- 46. Nikonova E, Mukherjee A, Kamble K, Barz C, Nongthomba U, Spletter ML: **Rbfox1 is required for myofibril development and maintaining fiber type-specific isoform expression in Drosophila muscles**. *Life science alliance* 2022, **5**(4).
- 47. Schnorrer F, Schonbauer C, Langer CC, Dietzl G, Novatchkova M, Schernhuber K, Fellner M, Azaryan A, Radolf M, Stark A *et al*: **Systematic genetic analysis of muscle morphogenesis and function in Drosophila**. *Nature* 2010, **464**(7286):287-291.
- 48. Kao SY, Nikonova E, Ravichandran K, Spletter ML: **Dissection of Drosophila melanogaster Flight Muscles for Omics Approaches**. In: *Journal of visualized experiments*. 20191017 edn; 2019.
- 49. Kao SY, Nikonova E, Chaabane S, Sabani A, Martitz A, Wittner A, Heemken J, Straub T, Spletter ML: A Candidate RNAi Screen Reveals Diverse RNA-Binding Protein Phenotypes in Drosophila Flight Muscle. *Cells* 2021, **10**(10).
- 50. Lence T, Akhtar J, Bayer M, Schmid K, Spindler L, Ho CH, Kreim N, Andrade-Navarro MA, Poeck B, Helm M *et al*: **m6A modulates neuronal functions and sex determination in Drosophila**. *Nature* 2016, **540**(7632):242-247.
- 51. Sandmann T, Jensen LJ, Jakobsen JS, Karzynski MM, Eichenlaub MP, Bork P, Furlong EE: A temporal map of transcription factor activity: mef2 directly regulates target genes at all stages of muscle development. Developmental cell 2006, 10(6):797-807.
- 52. Yao KM, White K: Neural specificity of elav expression: defining a Drosophila promoter for directing expression to the nervous system. *Journal of neurochemistry* 1994, **63**(1):41-51.
- 53. Duffy JB: **GAL4 system in Drosophila: a fly geneticist's Swiss army knife**. *Genesis* 2002, **34**(1-2):1-15.
- 54. Sarov M, Barz C, Jambor H, Hein MY, Schmied C, Suchold D, Stender B, Janosch S, K JV, Krishnan RT *et al*: **A genome-wide resource for the analysis of protein localisation in Drosophila**. *Elife* 2016, **5**.

55. Rai M, Katti P, Nongthomba U: **Drosophila Erect wing (Ewg) controls mitochondrial fusion during muscle growth and maintenance by regulation of the Opa1-like gene.** *Journal of cell science* 2014, **127**(Pt 1):191-203.

- 56. Hallmann K, Kudin AP, Zsurka G, Kornblum C, Reimann J, Stuve B, Waltz S, Hattingen E, Thiele H, Nurnberg P et al: Loss of the smallest subunit of cytochrome c oxidase, COX8A, causes Leigh-like syndrome and epilepsy. Brain: a journal of neurology 2016, 139(Pt 2):338-345.
- 57. Alessia Soldano LW, Chiara Paolantoni, Sara Longhi, Miriam M. Mulorz, Tina Lence, Hans-Hermann Wessels, Giuseppe Aiello, Michela Notarangelo, FX Reymond Sutandy, Marion Scheibe, Raghu R. Edupuganti, Anke Busch, Martin M. Möckel, Michiel Vermeulen, Falk Butter, Julian König, Uwe Ohler, Christoph Dieterich, Alessandro Quattrone, Jean-Yves Roignant: The m6A reader Ythdf restricts axonal growth in Drosophila through target selection modulation of the Fragile X mental retardation protein. In., vol. 40. The EMBO journal: EMBO press; 2021.
- 58. Worpenberg L, Paolantoni C, Longhi S, Mulorz MM, Lence T, Wessels HH, Dassi E, Aiello G, Sutandy FXR, Scheibe M *et al*: Ythdf is a N6-methyladenosine reader that modulates Fmr1 target mRNA selection and restricts axonal growth in Drosophila. *Embo journal* 2021, **40**(4).
- 59. Tina Lence JA, Marc Bayer, Katharina Schmid, Laura Spindler, Cheuk Hei Ho, Nastasja Kreim, Miguel A. Andrade-Navarro, Burkhard Poeck, Mark Helm & Jean-Yves Roignant **m6A modulates neuronal functions and sex determination in Drosophila**. *Nature* 2016, **540**:242-247.
- 60. Atlas of Drosophila development [https://www.sdbonline.org/sites/fly/atlas/00atlas.htm]
- 61. Ayme-Southgate A, Bounaix C, Riebe TE, Southgate R: **Assembly of the giant protein projectin during myofibrillogenesis in Drosophila indirect flight muscles**. *BMC Cell Biology* 2004, **5**:17.
- 62. Beall CJ, Sepanski MA, Fyrberg EA: **Genetic dissection of Drosophila myofibril formation: effects of actin and myosin heavy chain null alleles**. *Genes Development* 1989, **3**(2):131-140.
- 63. Reedy MC, Bullard B, Vigoreaux JO: Flightin is essential for thick filament assembly and sarcomere stability in Drosophila flight muscles. *Journal of cell biology* 2000, **151**(7):1483-1500.
- 64. Kittel RJ, Wichmann C, Rasse TM, Fouquet W, Schmidt M, Schmid A, Wagh DA, Pawlu C, Kellner RR, Willig KI *et al*: **Bruchpilot promotes active zone assembly, Ca2+channel clustering, and vesicle release**. *Science* 2006, **312**(5776):1051-1054.
- 65. Roos J, Hummel T, Ng N, Klambt C, Davis GW: **Drosophila Futsch regulates synaptic** microtubule organization and is necessary for synaptic growth. *Neuron* 2000, **26**(2):371-382.
- 66. Kuo YW, Trottier O, Mahamdeh M, Howard J: **Spastin is a dual-function enzyme that severs microtubules and promotes their regrowth to increase the number and mass of microtubules**. *Proceedings of the national academy of science of the united states of America* 2019, **116**(12):5533-5541.
- 67. Ayme-Southgate A, Saide J, Southgate R, Bounaix C, Cammarato A, Patel S, Wussler C: In indirect flight muscles Drosophila projectin has a short PEVK domain, and its NH2-terminus is embedded at the Z-band. Journal of Muscle Research and Cell Motility 2005, 26(6-8):467-477.
- 68. Moore JR, Vigoreaux JO, Maughan DW: **The Drosophila projectin mutant, bentD, has** reduced stretch activation and altered indirect flight muscle kinetics. *Journal of Muscle Research and Cell Motility* 1999, **20**(8):797-806.
- 69. Kan L, Grozhik AV, Vedanayagam J, Patil DP, Pang N, Lim KS, Huang YC, Joseph B, Lin CJ, Despic V et al: The m(6)A pathway facilitates sex determination in Drosophila. Nature Communications 2017, 8.

70. Lancaster CL, Yalamanchili PS, Goldy JN, Leung SW, Corbett AH, Moberg KH: The RNA-binding protein Nab2 regulates levels of the RhoGEF Trio to govern axon and dendrite morphology. *Molecular biology of the cell* 2024, **35**(8).

- 71. Syme DA, Josephson RK: **How to build fast muscles: synchronous and asynchronous designs**. *Integrative and comparative biology* 2002, **42**(4):762-770.
- 72. Mukund K, Subramaniam S: **Skeletal muscle: A review of molecular structure and function, in health and disease**. *Wiley interdisciplinary reviews* 2020, **12**(1).
- 73. Block GJ, Petek LM, Narayanan D, Amell AM, Moore JM, Rabaia NA, Tyler A, van der Maarel SM, Tawil R, Filippova GN et al: Asymmetric bidirectional transcription from the FSHD-causing D4Z4 array modulates DUX4 production. PLOS One 2012, 7(4).
- 74. Ganassi M, Zammit PS: Involvement of muscle satellite cell dysfunction in neuromuscular disorders: Expanding the portfolio of satellite cell-opathies. European journal of translational myology 2022, 32(1).
- 75. Petrosino JM, Hinger SA, Golubeva VA, Barajas JM, Dorn LE, Iyer CC, Sun HL, Arnold WD, He C, Accornero F: **The m(6)A methyltransferase METTL3 regulates muscle maintenance and growth in mice**. *Nature Communications* 2022, **13**(1):168.
- 76. Dorn LE, Lasman L, Chen J, Xu X, Hund TJ, Medvedovic M, Hanna JH, van Berlo JH, Accornero F: **The N(6)-Methyladenosine mRNA Methylase METTL3 Controls Cardiac Homeostasis and Hypertrophy**. *Circulation* 2019, **139**(4):533-545.
- 77. Gheller BJ, Blum JE, Fong EHH, Malysheva OV, Cosgrove BD, Thalacker-Mercer AE: A defined N6-methyladenosine (m(6)A) profile conferred by METTL3 regulates muscle stem cell/myoblast state transitions. Cell death discovery 2020, 6(1):95.
- 78. Zhao T, Zhao R, Yi X, Cai R, Pang W: **METTL3 promotes proliferation and myogenic differentiation through m(6)A RNA methylation/YTHDF1/2 signaling axis in myoblasts**. *Life sciences* 2022, **298**.
- 79. Liang Y, Han H, Xiong Q, Yang C, Wang L, Ma J, Lin S, Jiang YZ: **METTL3-Mediated** m(6)A Methylation Regulates Muscle Stem Cells and Muscle Regeneration by Notch Signaling Pathway. Stem Cells International 2021(Special Issue).
- 80. Tan B, Zeng J, Meng F, Wang S, Xiao L, Zhao X, Hong L, Zheng E, Wu Z, Li Z et al: Comprehensive analysis of pre-mRNA alternative splicing regulated by m6A methylation in pig oxidative and glycolytic skeletal muscles. *BMC Genomics* 2022, 23(1):804.
- 81. Achour C, Bhattarai DP, Groza P, Roman AC, Aguilo F: **METTL3 regulates breast** cancer-associated alternative splicing switches. *Oncogene* 2023, **42**(12):911-925.
- 82. Xu K, Yang Y, Feng GH, Sun BF, Chen JQ, Li YF, Chen YS, Zhang XX, Wang CX, Jiang LY et al: Mettl3-mediated m(6)A regulates spermatogonial differentiation and meiosis initiation. Cell research 2017, 27(9):1100-1114.
- 83. Roignant JY, Soller M: **m(6)A in mRNA: An Ancient Mechanism for Fine-Tuning Gene Expression**. *Trends in genetics* 2017, **33**(6):380-390.
- 84. Yuhan Qin LL, Erfei Luo, Jiantong Hou, Gaoliang Yan, Dong Wang, Yong Qiao, and Chengchun Tang: Role of m6A RNA methylation in cardiovascular disease (Review). International journal of molecular medicine 2020, 46(6):1958-1972.

Appendix 73

Appendix

Mass Spec results for sarcomere specific proteins

| | | | • | | | • | • | | | |
|------------|------------------|--------------------------------------|--------------------------------|------------------------|--------------------------------|--------------------------------|------------------------------------|------------------------------------|------------------------------------|------------------------------------|
| Gene name | P value (log) | Difference Mutant vs. Wildtype | LFQ inten- sity Mutant 1 | LFQ intensity Mutant 2 | LFQ inten- sity Mutant 3 | LFQ inten- sity Mutant 4 | LFQ inten- sity Wild- type 1 | LFQ inten- sity Wild- type 2 | LFQ inten- sity Wild- type 3 | LFQ inten- sity Wild- type 4 |
| wupA | 1.51298761 | 2.68943548 | 27.3600121 | 26.9054089 | 24 | 28.492321 | 24 | 24 | 24 | 24 |
| parvin | 1.77046056 | 2.61506367 | 27.5074863 | 27.5694981 | 27.3476486 | 27.2152119 | 24 | 24 | 24 | 27.1795902 |
| TpnC41C | 0.7578083 | 2.4800601 | 31.2266483 | 29.4435387 | 32.0211525 | 31.3304195 | 29.9411182 | 30.4016171 | 24 | 29.7587833 |
| TpnC25D | 0.74669054 | 2.27372122 | 28.3733501 | 28.0682011 | 24 | 28.6954117 | 24 | 28.042078 | 24 | 24 |
| Mhc | 1.09561062 | 2.19587088 | 30.3305264 | 34.0319862 | 30.5992127 | 32.3605042 | 29.0900269 | 30.3146248 | 28.2570095 | 30.8770847 |
| Zasp52 | 4.62926254 | 1.94394112 | 25.9016399 | 25.5867481 | 26.3906231 | 25.8967533 | 24 | 24 | 24 | 24 |
| Ilk | 1.25729165 | 1.76131821 | 27.3548946 | 26.8325558 | 26.5403042 | 27.241909 | 26.7124043 | 24 | 24 | 26.2119865 |
| TpnC73F | 0.72322748 | 1.6871686 | 28.9566803 | 29.7473202 | 28.1580296 | 28.7267647 | 27.9415093 | 28.8753433 | 24 | 28.0232678 |
| Lmpt | 0.44805845 | 1.65525389 | 29.1234913 | 30.6242714 | 31.286314 | 29.2221413 | 31.414175 | 29.327488 | 24 | 28.8935394 |
| Mlp84B | 1.11417938 | 1.49654436 | 27.6360951 | 27.689991 | 27.4708824 | 27.3143215 | 26.3055134 | 27.1033955 | 26.7162037 | 24 |
| Tm1 | 0.33180333 | 1.46251917 | 29.7269421 | 28.6643124 | 24 | 28.891571 | 28.6656342 | 24 | 28.7671146 | 24 |
| Zasp66 | 2.84068827 | 1.22836208 | 31.758276 | 31.8956928 | 32.065033 | 32.3142204 | 30.6667023 | 30.3394737 | 31.2229691 | 30.8906288 |
| rhea | 4.83667004 | 1.21154213 | 28.5343781 | 28.8431702 | 28.6778812 | 28.7918491 | 27.4402351 | 27.5694256 | 27.3468037 | 27.6446457 |
| Pax | 4.18310106 | 1.15101767 | 27.3530445 | 27.5816155 | 27.2571888 | 27.4438744 | 26.0152721 | 26.4555702 | 26.2099056 | 26.3509045 |
| tmod | 3.46005639 | 1.10278082 | 29.5449524 | 29.3693619 | 29.4098129 | 29.3129177 | 28.2008362 | 27.9823418 | 28.6607475 | 28.3819962 |
| Act57B | 0.71783921 | 0.99925709 | 32.7331963 | 30.2255001 | 32.4118271 | 32.929718 | 31.5007114 | 31.5442066 | 30.497242 | 30.7610531 |
| Mf | 1.8613884 | 0.95730019 | 34.5749741 | 33.5117111 | 34.4034348 | 34.1855621 | 33.3048401 | 32.8358078 | 33.5603561 | 33.1454773 |
| Prm | 2.7592242 | 0.85669041 | 33.095974 | 33.4270477 | 33.3406944 | 33.5475426 | 32.6708832 | 32.165638 | 32.7256584 | 32.4223175 |
| Msp300 | 4.40567066 | 0.80465365 | 31.6042595 | 31.8246422 | 31.5797005 | 31.5122032 | 30.8440094 | 30.783083 | 30.9098492 | 30.7652493 |
| Act79B | 2.35551174 | 0.73891258 | 33.4572105 | 33.5459328 | 33.8683891 | 33.476532 | 32.7450295 | 32.9279366 | 33.1808739 | 32.5385742 |
| up | 0.80416316 | 0.57448864 | 32.4143753 | 31.5676498 | 32.9991531 | 32.9950981 | 31.678503 | 32.2054825 | 31.9348412 | 31.8594952 |
| Mlc1 | 0.87400868 | 0.55380726 | 34.9654656 | 36.0806198 | 35.4628601 | 35.2354927 | 34.7382202 | 34.4151955 | 34.9421387 | 35.4336548 |
| if | 0.98049614 | 0.54572678 | 27.2111321 | 27.8709717 | 27.5187092 | 26.817997 | 26.3359604 | 26.9244499 | 27.1823406 | 26.7931519 |
| beta-Spec | 2.38985472 | 0.52810574 | 33.3665886 | 33.5858688 | 33.2928276 | 33.1237831 | 32.7315598 | 32.8815613 | 32.6748047 | 32.9687195 |
| Mhc | 1.34324028 | 0.4956274 | 35.5319176 | 36.1796455 | 35.4872971 | 35.2856445 | 35.1501312 | 35.0441704 | 35.1014557 | 35.2062378 |
| Tm1 | 0.52802144 | 0.49130011 | 31.0297985 | 29.3812332 | 30.2831707 | 30.9942226 | 30.0758438 | 30.108738 | 29.3745327 | 30.1641102 |
| alpha-Spec | 1.77057409 | 0.4322772 | 31.0447254 | 31.014183 | 30.5817223 | 30.8769398 | 30.2826176 | 30.6559963 | 30.3832951 | 30.4665527 |
| Tm1 | 0.15721458 | 0.41906881 | 26.7662296 | 24 | 27.0068874 | 24 | 24 | 26.0310326 | 24 | 26.0658093 |
| Mlp60A | 0.0961933 | 0.40029097 | 24 | 29.0297852 | 24 | 24 | 24 | 24 | 24 | 27.4286213 |
| up | 0.92928163 | 0.3952961 | 33.0500565 | 33.5500679 | 33.4509583 | 33.866272 | 33.0392761 | 32.8220596 | 33.0082321 | 33.4666023 |
| stv | 0.33472192 | 0.37746954 | 26.08671 | 27.4780006 | 25.2736969 | 26.0848885 | 26.0486202 | 25.7718296 | 25.4689884 | 26.1239796 |
| Prm | 2.39533037 | 0.34732246 | 33.3202591 | 33.4935722 | 33.1691208 | 33.3826523 | 32.9861908 | 32.9318161 | 32.9601669 | 33.0981407 |
| chic | 0.11272922 | 0.32309198 | 26.7569733 | 27.0265427 | 24 | 24 | 24 | 26.4823151 | 26.0088329 | 24 |
| zormin | 0.89645061 | 0.32234573 | 28.9886665 | 28.6743164 | 28.8960533 | 28.3875122 | 28.4361095 | 28.1462765 | 28.3371773 | 28.7376022 |
| Act88F | 1.81844623 | 0.3030138 | 36.428875 | 36.8015976 | 36.5692139 | 36.4900208 | 36.2485924 | 36.1701965 | 36.3238182 | 36.3350449 |
| Mhc | 0.06931339 | 0.30111361 | 28.2072735 | 28.7690697 | 24 | 28.7103348 | 28.0140362 | 28.4003964 | 24 | 28.067791 |
| fln | 0.97460797 | 0.29766369 | 34.6609764 | 35.1147766 | 34.9319191 | 34.6407585 | 34.7557831 | 34.2423248 | 34.5697212 | 34.5899468 |
| sls | 2.07208876 | 0.27155018 | 32.3001556 | 32.1935463 | 32.3672905 | 32.3609505 | 32.0516777 | 31.8755493 | 32.1541824 | 32.0543327 |
| wupA | 1.0094717 | 0.26801872 | 34.5442658 | 34.543747 | 34.9414406 | 34.6210213 | 34.2237473 | 34.3665237 | 34.6774521 | 34.3106766 |
| Strn-Mlck | 2.55329331 | 0.25101185 | 34.3533058 | 34.2825089 | 34.3728905 | 34.4460373 | 34.1325455 | 33.9971542 | 34.1578293 | 34.1631661 |
| Mhc | 1.28925616 | 0.21814346 | 36.1748161 | 36.1829033 | 36.3443031 | 36.1956825 | 36.0032196 | 35.7832451 | 36.152874 | 36.0857925 |
| TpnC4 | 0.62040315 | 0.16947651 | 33.9413109 | 34.3095245 | 34.2397652 | 34.4022293 | 33.8347931 | 34.2322083 | 34.1092987 | 34.0386238 |

Appendix 74

| Gene name | P value (log) | Difference Mutant vs. Wildtype | LFQ inten- sity Mutant 1 | LFQ inten- sity Mutant 2 | LFQ inten- sity Mutant 3 | LFQ inten- sity Mutant 4 | LFQ inten- sity Wild- type 1 | LFQ inten- sity Wild- type 2 | LFQ inten- sity Wild- type 3 | LFQ inten- sity Wild- type 4 |
|-----------------|--------------------------|--------------------------------------|--------------------------------|--------------------------------|--------------------------------|--------------------------------|------------------------------------|------------------------------------|------------------------------------|------------------------------------|
| SERCA | 0.52346419 | 0.16900349 | 33.5782394 | 33.1299667 | 33.6185074 | 33.5922318 | 33.1139946 | 33.2047081 | 33.5179405 | 33.4062882 |
| Zasp52 | 0.04269839 | 0.14631558 | 27.7378273 | 27.3778248 | 27.2200203 | 24 | 27.2879772 | 27.0078507 | 24 | 27.4545822 |
| Actn | 1.29014151 | 0.13796711 | 33.5685349 | 33.5653572 | 33.5198135 | 33.5944595 | 33.5074616 | 33.2636032 | 33.471817 | 33.4534149 |
| hts | 0.3256251 | 0.11687899 | 31.3484726 | 30.8405609 | 30.8203888 | 30.8715153 | 30.8798637 | 30.9980621 | 30.6085835 | 30.9269123 |
| Mlc2 | 0.23404638 | 0.10820293 | 35.0122604 | 34.4397965 | 35.2792931 | 35.1119041 | 34.852478 | 34.8746338 | 34.7432442 | 34.9400864 |
| Mp20 | 0.11518868 | 0.08267546 | 28.7853451 | 28.5383816 | 28.2122459 | 28.8106308 | 28.7354412 | 28.6277371 | 27.8317719 | 28.8209515 |
| TpnC47D | 0.0197847 | 0.06585693 | 24 | 24 | 24 | 27.3286018 | 24 | 27.0651741 | 24 | 24 |
| bt | 0.20543382 | 0.0610199 | 32.9348564 | 32.5974159 | 33.0284996 | 32.9262581 | 32.86129 | 32.6461372 | 32.9766121 | 32.7589111 |
| Zasp52 | 0.12783821 | 0.03174591 | 33.0956574 | 33.1485863 | 33.1708832 | 33.1031189 | 33.1427269 | 32.8666229 | 33.3082352 | 33.0736771 |
| wupA | 0.02508881 | 0.02729464 | 28.0809593 | 27.8919182 | 27.8490009 | 27.2088089 | 27.0263329 | 27.4947262 | 28.542408 | 27.8580418 |
| Tm1 | 0.02514611 | 0.01014137 | 34.834507 | 34.7028008 | 35.1524773 | 35.0973015 | 34.8493118 | 34.7361527 | 35.0514832 | 35.1095734 |
| up | 0.00476567 | 0.0014286 | 34.7720032 | 34.5107651 | 34.6826935 | 34.9037399 | 34.7827339 | 34.5462799 | 34.7537918 | 34.7806816 |
| Tm1 | 0 | 0 | 24 | 24 | 24 | 24 | 24 | 24 | 24 | 24 |
| tmod | 0 | 0 | 24 | 24 | 24 | 24 | 24 | 24 | 24 | 24 |
| bt | 0 | 0 | 24 | 24 | 24 | 24 | 24 | 24 | 24 | 24 |
| Msp300 | 0 | 0 | 24 | 24 | 24 | 24 | 24 | 24 | 24 | 24 |
| Mhc | 0 | 0 | 24 | 24 | 24 | 24 | 24 | 24 | 24 | 24 |
| SERCA | 0 | 0 | 24 | 24 | 24 | 24 | 24 | 24 | 24 | 24 |
| Lasp | 0 | 0 | 24 | 24 | 24 | 24 | 24 | 24 | 24 | 24 |
| Tm1 | 0 | 0 | 24 | 24 | 24 | 24 | 24 | 24 | 24 | 24 |
| Zasp66 | 0 | 0 | 24 | 24 | 24 | 24 | 24 | 24 | 24 | 24 |
| Zasp67 RyR | 0.00191539 | 0 - 0.00952959 | 28.669323 | 24 | 24 | 24 | 24 | 24 | 28.7074413 | 24 |
| Arp3 | 0.01168319 | -0.022892 | 24 | 24 | 24 | 25.8204823 | 24 | 24 | 24 | 25.9120503 |
| | | - | | | | | | | | |
| Mlp60A | 0.17775536 | 0.06187534 | 30.3823681 | 30.3303127 | 30.6743832 | 30.310297 | 30.4260235 | 30.2266483 | 30.7243595 | 30.567831 |
| Unc-89 | 0.34623561 | 0.07378006 | 31.6434498 | 31.9489346 | 31.7465115 | 31.6194687 | 31.9258862 | 31.6734982 | 31.8168068 | 31.8372936 |
| RyR | 0.39761557 | -0.0779953 | 30.7166939 | 31.0442696 | 30.7505493 | 30.7290688 | 30.8904114 | 30.7914925 | 30.9639587 | 30.9067001 |
| 72cn67 | 0.22894723 | -0.1106863 | 34.8245392 | 34.1449776 | 34.8105774 | 34.9570122 | 34.6150017 32.0719528 | 34.7721977 | 34.9114838 | 34.8811684 |
| Zasp67 CanB2 | 0.72191525 0.37242398 | 0.19101906 - 0.19749403 | 31.6340008 27.5687008 | 31.7323875 26.7242947 | 31.779604 27.2701721 | 32.1798821 27.4574814 | 27.6620731 | 31.9608555 27.6927204 | 32.1311493 27.1470528 | 31.925993 27.3087788 |
| Strn-Mlck | 0.95497691 | 0.22316313 | 28.6012325 | 28.0923481 | 28.487154 | 28.3068256 | 28.5066547 | 28.6306896 | 28.7003479 | 28.5425205 |
| Bsg | 0.37537575 | 0.27148151 | 30.1554489 | 28.9677143 | 30.0240612 | 30.0220776 | 29.8059502 | 29.8769531 | 30.4720841 | 30.1002407 |
| Chd64 | 0.87177602 | - 0.42488623 | 29.145134 | 28.5812206 | 28.2391796 | 28.7222099 | 29.3037586 | 29.4153042 | 28.9329777 | 28.7352486 |
| Prm | 0.13128421 | - 0.42523146 | 27.6539669 | 29.0485878 | 29.2169476 | 24 | 27.7517471 | 27.6787548 | 28.2762203 | 27.9137058 |
| Mf | 0.15222329 | - 0.47282744 | 24 | 27.5057449 | 24 | 26.9582577 | 24 | 26.7423973 | 26.3008423 | 27.3120728 |
| Lmpt | 2.44925156 | - 0.48757839 | 29.0625515 | 29.2636719 | 29.2103424 | 29.0858288 | 29.6166153 | 29.4501629 | 29.8986511 | 29.6072788 |
| cpb | 0.21558928 | - 0.50790167 | 26.7480412 | 24 | 26.1985798 | 24 | 25.942728 | 26.709383 | 24 | 26.3261166 |
| Tm2 | 0.61502248 | 0.55331516 | 33.6229858 | 32.0189972 | 33.9242401 | 33.4950028 | 33.7064591 | 33.874176 | 33.8821259 | 33.8117256 |
| Hsp83 | 2.11661594 | - 0.75894737 | 29.7003155 | 30.5506878 | 30.1749802 | 29.8349228 | 30.8393612 | 30.8845291 | 30.7356987 | 30.8371067 |

Appendix 75

| Gene name | P value (log) | Difference Mutant vs. Wildtype | LFQ inten- sity Mutant 1 | LFQ intensity Mutant 2 | LFQ inten- sity Mutant 3 | LFQ inten- sity Mutant 4 | LFQ inten- sity Wild- type 1 | LFQ inten- sity Wild- type 2 | LFQ inten- sity Wild- type 3 | LFQ inten- sity Wild- type 4 |
|-----------|------------------|--------------------------------------|--------------------------------|------------------------|--------------------------------|--------------------------------|------------------------------------|------------------------------------|------------------------------------|------------------------------------|
| flr | 0.55255618 | -0.9004159 | 26.8129883 | 24 | 27.3387508 | 26.7645855 | 27.1547985 | 27.043747 | 27.347311 | 26.9721317 |
| tn | 3.56471927 | - 0.95894671 | 26.3828945 | 26.8389397 | 26.5098591 | 26.8574486 | 27.7176418 | 27.5958386 | 27.5092239 | 27.6022244 |
| unc-45 | 0.81129848 | -0.9700861 | 25.0115433 | 27.7730389 | 26.5087414 | 26.7423973 | 27.8578053 | 27.6557407 | 27.075716 | 27.3268032 |
| mys | 0.29846376 | - 1.01912737 | 27.786562 | 24 | 24 | 27.5277576 | 28.0493164 | 27.3235416 | 24 | 28.017971 |
| Msp300 | 0.86266266 | -1.2848444 | 24 | 24 | 24 | 24 | 24 | 26.311779 | 26.8275986 | 24 |
| Dg | 1.59439797 | - 1.46490765 | 24 | 24 | 24 | 24 | 26.1757145 | 24 | 25.9238167 | 25.7600994 |
| sls | 0.70251925 | - 1.63236046 | 28.3973389 | 24 | 28.4722385 | 28.6244984 | 28.7570038 | 29.0233746 | 29.0625515 | 29.1805878 |
| sals | 2.18082398 | - 2.52025461 | 26.506321 | 25.8986454 | 26.4153194 | 24 | 28.4113483 | 28.4822006 | 27.60569 | 28.4020653 |

Significant probes are written in bold letters

Acknowledgements 76

Acknowledgements

I sincerely want to thank Professor Ladurner for supervising my work, giving me access to all the reagents and facilities and thus making this project possible.

Also, I would like to thank Professor Kiebler and Professor Becker for being on my supervision committee and all their valuable advice and help.

Of course, I cordially want to thank Professor Maria Spletter for having me in her scientific group. I really value all that I have learned from her and in that time. Without her impulses, ideas, explanations and help with interpreting results and designing future steps, this project would have been impossible. Maria Spletter also did the bioinformatics for the MassSpec, qPCR and mRNA sequencing experiments.

Speaking of those experiments, I would like to thank the LaFuga Core Facility for running and the BMC Bioinformatics Core Facility and in particular Dr. Tobias Straub for help with analyzing mRNA sequencing experiments, as well as the BMC Proteomics Core Facility and in particular Dr. Ignasi Forne for conducting the MassSpec and helping with proteomics analysis.

Of course, I have to thank Sandra Esser for her work and the countless hours she invested into this project. Sandra Esser did the electrophoresis, dot blot and western blot experiments. Furthermore, she collected the probes for the MassSpec and PCR experiments.

I would also like to thank Shao-Yen Kao and Elena Nikonova for always having an open ear for me and showing me around in the laboratory. I also appreciate their training regarding dissections and biochemical procedures very much.

Also, I would like to thank Marc Canela Grimau for contributing the pupa lethality and jumping experiments for showing, that the used NIG-hairpin is in fact target specific.

Last but not least I want to thank Maria Armero for repeating certain experiments to confirm my findings.

I had a really good time and will miss you all!

Confirmation of congruency



LUDWIG-MAXIMILIANS-UNIVERSITÄT MÜNCHEN





Eidesstattliche Versicherung

Heemken, Jakob

Name, Vorname

Ich erkläre hiermit an Eides statt, dass ich die vorliegende Dissertation mit dem Titel:

Mettl3 is required cell intrinsically in both muscle and neurons for development of functional flight muscle

selbständig verfasst, mich außer der angegebenen keiner weiteren Hilfsmittel bedient und alle Erkenntnisse, die aus dem Schrifttum ganz oder annähernd übernommen sind, als solche kenntlich gemacht und nach ihrer Herkunft unter Bezeichnung der Fundstelle einzeln nachgewiesen habe.

Ich erkläre des Weiteren, dass die hier vorgelegte Dissertation nicht in gleicher oder in ähnlicher Form bei einer anderen Stelle zur Erlangung eines akademischen Grades eingereicht wurde.

München, 5.10.2025

Ort, Datum

Jakob Heemken

Unterschrift Doktorandin bzw. Doktorand

Publications 78

Publications

A candidate RNAi screen reveals diverse RNA-binding protein phenotypes in *Drosophila* flight muscle.

(Cells, 2021 by Kao, Nikonova, Chaabane, Sabani, Martitz, Wittner, Heemken, Straub, Spletter; https://pubmed.ncbi.nlm.nih.gov/34685485/)